Characterizing Low-Frequency Qubit Noise

Filip Wudarski,[1,2] Yaxing Zhang,[3] Alexander N. Korotkov,[3,4] A.G. Petukhov,[3] and M.I. Dykman[5,*]

[1] *Quantum Artificial Intelligence Laboratory, Exploration Technology Directorate, NASA Ames Research Center, Moffett Field, California 94035, USA*

[2] *USRA Research Institute for Advanced Computer Science (RIACS), Mountain View, California 94043, USA*

[3] *Google Research, Mountain View, California 94043, USA*

[4] *Department of Electrical Engineering, University of California, Riverside, California 92521*

[5] *Department of Physics and Astronomy, Michigan State University, East Lansing, Michigan 48824, USA*

(Received 27 September 2022; revised 26 April 2023; accepted 10 May 2023; published 22 June 2023)

Fluctuations of the qubit frequencies are one of the major problems to overcome on the way to scalable quantum computers. Of particular importance are fluctuations with a correlation time that exceeds the decoherence time due to decay and dephasing by fast processes. The statistics of the fluctuations can be characterized by measuring the correlators of the outcomes of periodically repeated Ramsey measurements. We describe qubit dynamics during repeated measurements and evaluate the two-time correlator for noise from two-level systems and two- and three-time correlators for Gaussian noise. The explicit expressions for the correlators are compared with simulations. We find that, even though the three-time correlators for noise from two-level systems and for Gaussian noise are generally significantly different, already ten two-level systems can mimic Gaussian noise provided they are symmetric. This is not the case for asymmetric systems.

DOI: 10.1103/PhysRevApplied.19.064066

I. INTRODUCTION

Decoherence, and in particular qubit phase fluctuations due to the qubit frequency noise, are one of the major obstacles faced by quantum computing. This makes it important to understand the mechanism of the frequency noise. To this end, much work has focused on the analysis of the noise spectra; cf. Refs. [1–20] and the references therein. For condensed-matter-based qubits, the analysis is frequently based on the assumption that the noise is Gaussian, as it comes from many independent sources, each of which is weakly coupled to a qubit. This assumption does not necessarily apply, particularly for low-frequency noise [21–24]. The latter is often thought to result from random hopping between the states of two-level systems (TLSs) coupled to a qubit. However, TLS-induced frequency noise is generally non-Gaussian [25–31], reminiscent of the fluctuations studied in nuclear magnetic resonance and leading to the spectral diffusion; see Refs. [32,33].

To characterize the noise that causes qubit decoherence, it is important to know not just the noise spectrum, but also its statistics. The problem has attracted considerable interest [20,34–39]. A natural approach is to characterize higher-order spectral moments of the noise. For zero-mean Gaussian noise, all moments are expressed in terms of the second moment. A deviation from the corresponding interrelation between the moments is a signature of the noise being non-Gaussian.

For frequency noise in mesoscopic vibrational systems, higher-order moments were studied in Refs. [40,41]. For frequency noise in qubits, the possibility to measure the third spectral moment (the bispectrum) was demonstrated in Ref. [38] by building on the approach [36] of evaluating noise polyspectra. The approach is based on using a large number of distinct sequences of refocusing pulses during Ramsey measurements. The data acquisition time is therefore limited by the lifetime of a qubit. A similar constraint also refers to the results on the three-time correlator presented in Ref. [42] where projective measurements were used instead of refocusing. Higher-order correlation functions of a spin qubit in an optically active quantum dot were studied using multiple interpulse intervals, with the overall measurement duration also limited by the qubit lifetime [43]. This latter work is directly related to the field of optical spin noise spectroscopy, where higher-order statistics of the noise plays an important role [34,44].

In the present paper we develop means for studying, in a single series of repeated measurements, the statistics of qubit noise with frequencies that are not limited by the reciprocal qubit lifetime. This is a key distinction from the previous work. The relevant low-frequency noise plays a critical role in the operation of a quantum computer.

*dykmanm@msu.edu

In particular, it limits the time over which repeated gate operations can be reliably performed on a qubit. The corresponding timescale and the noise mechanism depend on the qubit implementation. For example, for the currently used superconducting qubits, the timescale of interest is in the range of 0.01–10 ms; one of the major sources of fluctuations on this timescale is the coupling to TLSs. TLSs are an important source of low-frequency noise in other types of qubits as well.

Our approach is not limited to noise frequencies from below. Even though the approach applies, the statistics of very slow frequency noise can be analyzed directly from the time dependence of the qubit frequency. Such time dependence has been resolved in several experiments; cf. Refs. [4,45,46]. Very slow noise can be caused by various physical mechanisms; for example, for superconducting qubits, those can be cosmic rays or high-energy photons [47,48]. The analysis of such noise is beyond the scope of the present paper.

Our goal is to develop an analytical theory of the effects of the noise statistics. The theory should be sufficiently general to account for different types of noise, including both Gaussian and non-Gaussian noise, and for the qubit dynamics involved in the measurements. We also aim at performing numerical simulations, which can be compared with the theory and in some cases can go beyond the range where analytical results can be obtained or become too cumbersome.

We study the first three correlators of the qubit frequency noise. Knowing three correlators is sufficient for distinguishing Gaussian from non-Gaussian noise. The study can be conveniently done by periodically repeating Ramsey measurements (cf. Ref. [5]), but going beyond noise spectroscopy. The actual correlators directly accessible to the experiment are the correlators of the measurement outcomes, and these are the characteristics we study. For the low-frequency noise, it is advantageous to analyze the results primarily in the time rather than the frequency domain, particularly where we are not limited to the effects of the lowest order in the noise intensity.

The measurement periodicity, which underlies our approach, is advantageous in that it allows one to find multiple-time correlators from a single sequence of repeated measurements. Indeed, the correlators of the outcomes separated by given numbers of periods can be obtained directly. The averaging is performed just by "sliding" along the data array keeping given distances between the data points.

One of the questions of general interest that we address is to understand the conditions where the TLS noise mimics Gaussian noise. An obvious answer is that it happens where there are many independent TLSs weakly coupled to the qubit, so as to meet the central limit theorem condition. On the other hand, there is an argument that the number of states of the TLS-induced noise scales with the number of TLSs N_{TLS} as $2^{N_{\mathrm{TLS}}}$, so that the actual number of TLSs does not necessarily have to be large. Comparing the correlators of the measurement outcomes should allow one to find how close the TLS noise comes to being Gaussian depending on the coupling and the parameters of TLSs.

Identifying the mechanism of classical non-Gaussian qubit noise based on its correlators is a hard problem, generally. Such noise is often a result of "processing" of Gaussian noise by nonlinear systems coupled to a qubit. The telegraph noise from TLSs is a familiar example. Indeed, in the standard model of TLSs [49–51] it results from interstate switching of a strongly nonlinear (two-state) system due to its coupling to a bosonic reservoir, with this reservoir itself being a source of Gaussian noise. Therefore, it is helpful to have a "map" of the outcomes of the measurements depending on the noise correlation and statistics for different types of noise sources.

A. The structure of the paper

We aim at studying the correlators of measurement outcomes for TLSs, analytically and via simulations. We also study correlation functions for three important types of Gaussian noise with a large correlation time: exponentially correlated noise, noise with a "profound color," i.e., with a comparatively narrow peak at nonzero frequency in the power spectrum, and $1/f$ -type noise.

The analytical calculations are fairly cumbersome. Therefore we separate the paper into three parts. The first part presents the results of the calculations and describes the simulations and the comparison of the theory and the simulations. The second part describes the theoretical approach that we develop. The details of the calculations and of the simulation algorithm are presented in the appendices.

The first part comprises Secs. II–VI. It presents, without a derivation, explicit general expressions for the correlators of the measurement outcomes. It also provides simplified versions of these expressions in various limiting cases. In Sec. II we describe the scheme of periodically repeated Ramsey measurements and define the two- and three-time correlation functions of the measurement outcomes. Section III summarizes the analytical results on the effect of coupling to TLSs. It gives the explicit expression for the two-time correlator and discusses the limiting cases of (i) weak coupling to the TLSs (in frequency units) compared to the TLS switching rates, (ii) short interval between the Ramsey pulses compared to the reciprocal coupling and switching rates, and (iii) strong coupling compared to the TLS switching rates.

Section IV provides explicit expressions for the two- and three-time correlators in the case of Gaussian noise. It shows how to do the measurements in the optimal way in order to distinguish Gaussian and non-Gaussian noise. The

parameters in the general expressions are evaluated for (i) exponentially correlated noise (with the Lorentzian power spectrum centered at $\omega = 0$), (ii) noise with "profound color," and (iii) $1/f$ -type noise.

In Sec. V we relate the discrete Fourier transform of the measurement outcomes to the noise power spectrum in the case where the noise is weak. In particular, we show that, generally, there is no one-to-one correspondence between the spectra. For completeness, we provide the relation between the centered two-time correlator of the measurement outcomes and the bispectrum often used in the analysis of non-Gaussian noise.

Section VI presents the results of the simulations and a detailed comparison of the theory and simulations for different types of noise. In particular, we study the manifestations of Gaussianity and non-Gaussianity of the noise. The results show the effects of (i) coupling to symmetric TLSs, for different numbers of TLSs and different coupling strengths, (ii) coupling to asymmetric TLSs, and (iii) the effects of exponentially correlated Gaussian noise and $1/f$ -type Gaussian noise.

In Sec. VII we derive a master equation for a qubit coupled to TLSs and driven by Gaussian noise and consider the qubit dynamics during the Ramsey measurement and the probability of the measurement outcome. In Sec. VIII we develop a method that allows us to find the two-time correlator of the outcomes for the TLS-induced noise. The approach is further developed in Sec. IX to analyze the effect of Gaussian noise on the one-, two-, and three-time correlators. Section X provides a summary of the results.

In Appendix A we provide an alternative method that makes it possible to find the correlator of the outcomes of repeated Ramsey measurements in the presence of telegraph noise. In Appendix B we describe the simulation algorithms. Other appendices provide some details of the calculations and present more results on the noise spectra and the correlators of the measurement outcomes.

II. THE CORRELATION FUNCTION OF MEASUREMENT OUTCOMES

We associate the operators acting on the qubit states with the Pauli operators $\sigma_{x,y,z}$ and the unit operator $\hat{I}_q$. The ground and excited states of the qubit are the eigenstates of σ_z. In the Bloch sphere representation they are $|0\rangle \equiv |\uparrow\rangle$ and $|1\rangle \equiv |\downarrow\rangle$, respectively. We consider a periodic sequence of Ramsey measurements sketched in Fig. 1 [4–6]. In the first Ramsey measurement the qubit, initially in state $|0\rangle$, is rotated at time $t = 0$ by $\pi/2$ around the y axis into state $(|0\rangle + |1\rangle)/\sqrt{2}$. At t_R it is rotated by $\pi/2$ around the y axis again and the occupation of state $|1\rangle$ is measured. After the measurement the qubit is reset to the ground state. The Ramsey measurements are then repeated with period $t_{\rm cyc}$, which we call the cycle period. For simplicity, we disregard the duration of the gate operations and the measurement as well as the gate and measurement errors. A similar sequence, but limited just to two measurements, was used in Ref. [52]. A two-measurement sequence does not allow studying the effects explored in this paper.

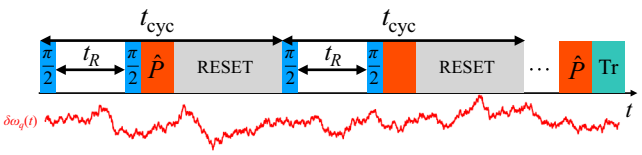

FIG. 1. Schematics of the Ramsey measurements. In each measurement qubit phase is accumulated over time t_R. The measurements are projective, $\hat{P} = |1\rangle\langle 1|$. They are repeated with period $t_{\rm cyc}$. After a measurement the qubit is reset to the ground state. Studied are two- and three-time correlators of the measurement outcomes. The jagged line at the bottom of the figure is a sketch of the qubit frequency fluctuations.

In a Ramsey measurement, the phase accumulated by the qubit over time t_R is compared with the phase accumulated over this time by a reference resonant signal. The accumulation of the phase difference θ is thus determined by fluctuations $\delta\omega_q(t)$ of the qubit frequency. These fluctuations are described by the Hamiltonian

$$H_{\rm fl} = -\tfrac{1}{2}\delta\omega_q(t)\sigma_z \qquad (\hbar = 1). \tag{1}$$

The random phase θ_k accumulated over a kth cycle, i.e., over the time interval $(kt_{\rm cyc}, kt_{\rm cyc} + t_R)$, is

$$\theta_k = \int_{kt_{\rm cyc}}^{kt_{\rm cyc}+t_R} \delta\omega_q(t)dt. \tag{2}$$

As seen from Eq. (2), fluctuations $\delta\omega_q(t)$ with a typical correlation time much shorter than t_R are largely averaged out. Periodic repetition of the Ramsey measurements allows revealing fluctuations with correlation times not only on the scale of t_R, but also on the scale determined by the cycle period $t_{\rm cyc}$. Of interest are zero-mean fluctuations, $\langle\delta\omega_q\rangle = 0$ (see, however, the discussion of the coupling to TLSs).

We assume that the system, including noise, is stationary. Then measurement outcomes only depend on the time interval between the measurements. We consider the expectation values of the outcomes $r_1, r_2(k)$, and $r_3(k,\ell)$ of obtaining "1" in a single measurement, obtaining "1" and "1" in two measurements separated by k cycles, and obtaining three "1"s in three measurements in which two measurements are separated from the first one by k and l cycles, respectively; for concreteness, we assume that $l > k \geq 1$. These expectation values are time correlators and are given by the correlation functions of the projection

operator $\hat{P} = (\hat{I}_q - \sigma_z)/2 \equiv |1\rangle\langle 1|$,

$$\begin{aligned} r_1 &= \mathrm{Tr}[\hat{P}(t_R^+)\rho(0^-)], \\ r_2(k) &= \mathrm{Tr}[\hat{P}(kt_{\mathrm{cyc}} + t_R^+)\hat{P}(t_R^+)\rho(0^-)], \end{aligned} \tag{3}$$

and

$$\begin{aligned} r_3(k,\ell) = \mathrm{Tr}[&\hat{P}(\ell t_{\mathrm{cyc}} + t_R^+)\hat{P}(kt_{\mathrm{cyc}} + t_R^+) \\ &\times \hat{P}(t_R^+)\rho(0^-)], \end{aligned} \tag{4}$$

where ρ is the density matrix of the system; $\hat{I}_q$ is the unit operator in the qubit space. Superscripts "+" and "−" of the time arguments indicate that the operator is respectively evaluated right after or right before the corresponding instant of time, i.e., right after or right before the gate operation performed at this time, $t^{\pm} \equiv t \pm \varepsilon$ with $\varepsilon \to +0$; in particular, 0^- is the time right before the rotation around the y axis at $t = 0$, whereas t_R^+ is the time right after the rotation at $t = t_R$. Clearly, r_1 is just the probability of obtaining "1" in a Ramsey measurement.

The traces in Eqs. (3) and (4) are calculated over the states of the qubit and the thermal reservoir coupled to the qubit, including the states of the TLSs if the TLSs play a role. The traces also imply averaging over the realizations of noise in the case where noise is a classical random force that modulates the qubit frequency.

The outcome of an nth Ramsey measurement x_n takes on value 1 or 0. Correlators $r_{1,2,3}$ are determined by the expectation values of these outcomes and their products,

$$\begin{aligned} r_1 = \mathbb{E}[x_n], \qquad r_2(k) = \mathbb{E}[x_{n+k}x_n], \\ r_3(k,\ell) = \mathbb{E}[x_{n+\ell}x_{n+k}x_n] \end{aligned} \tag{5}$$

Somewhat conditionally, we use $\mathbb{E}[\cdot]$ when referring to the expectation values, whereas for the results of statistical averaging based on analytical expressions, we use $\langle\cdot\rangle$. For classical Gaussian noise, correlators $r_3(k,\ell)$ are fully determined by r_1 and $r_2(k)$. We find the corresponding relations. If they do not hold, this indicates that *the noise is non-Gaussian*.

An advantageous feature of periodically repeated measurements is that the averaging is greatly simplified. Rather than repeating measurements for each k or each pair (k, l), one can use a single long series to find different correlators. For example,

$$\mathbb{E}[x_{n+k}x_n] \approx M^{-1}\sum_{n=1}^{M} x_{n+k}x_n.$$

Here M should be large; it should greatly exceed the correlation length of the sequence (formally, $M \to \infty$), but the expression applies for an arbitrary k. In contrast to $r_2(k)$ and $r_3(k,\ell)$, which give the time correlation functions for times kt_{cyc} and $(kt_{\mathrm{cyc}}, \ell t_{\mathrm{cyc}})$, respectively, r_1 is independent of t_{cyc} and can be obtained just as $M^{-1}\sum_n x_n$ for large M.

Along with $r_{2,3}$ we also consider centered correlators

$$\begin{aligned} \tilde{r}_2(k) &= \mathbb{E}[(x_{n+k} - r_1)(x_n - r_1)], \\ \tilde{r}_3(k,\ell) &= \mathbb{E}[(x_{n+\ell} - r_1)(x_{n+k} - r_1)(x_n - r_1)]. \end{aligned} \tag{6}$$

The discrete Fourier transforms of correlators $\tilde{r}_{2,3}$ give the spectrum and the bispectrum of the measurement outcomes; see Sec. V

In what follows we analytically calculate correlators $r_{1,2,3}$ and compare them with the results of simulating sequences x_n for several types of fluctuations. We typically simulate $N = 10^5$ cycles and average the results over 300 repetitions. This limits the noise correlation time we can reliably simulate to $\lesssim 10^4 t_{\mathrm{cyc}}$.

For a Ramsey measurement, the probability r_1 depends on the phase θ accumulated between the Ramsey pulses due to noise. For a given θ, the probability of obtaining "1" in a measurement is [53]

$$p(\theta) = \tfrac{1}{2}[1 + e^{-t_R/T_2}\cos(\phi_R + \theta)]. \tag{7}$$

For a random θ, probability r_1 is given by the mean value of $p(\theta)$. In Eq. (7), T_2^{-1} is the qubit decoherence rate due to fast, on a scale $\sim t_R$, decay and dephasing processes, which can usually be well described as Markovian. Phase ϕ_R mimics the phase accumulated due to the difference between the qubit frequency ω_q and the frequency of the reference signal ω_{ref},

$$\phi_R = (\omega_q - \omega_{\mathrm{ref}})t_R. \tag{8}$$

This phase can be (and frequently is) also added in a controlled way by a gate operation; see Eq. (57) below.

A note is due on the difference between the effects of TLSs on correlators of different orders. In the model of noninteracting TLSs that we consider, TLSs contribute to phase θ independently. The overall phase is a sum of these contributions. From Eq. (7), the value of r_1 is determined by $\langle\exp(i\theta)\rangle$ and can be calculated by multiplying the contributions of individual TLSs [25,26,28]. In contrast, r_2 and higher-order correlators should contain terms that decay as individual TLSs, their pairs, triples, etc. Therefore, these correlators may not be calculated as products of the contributions of individual TLSs.

III. DISPERSIVE COUPLING TO TWO-LEVEL SYSTEMS

We study two major mechanisms of qubit decoherence: classical fluctuations of the qubit frequency and the effect of coupling to TLSs. The level spacing of TLSs is assumed to be smaller than the qubit level spacing. In this case

there is no resonant energy exchange between the qubit and TLSs. The major effect of TLSs is to modulate the qubit frequency as TLSs switch between their states. The analysis is involved. Therefore we first provide the results, whereas their derivations are postponed until Secs. VII–IX.

A. Power spectrum of the qubit frequency noise

Qubit decoherence due to the dispersive qubit-to-TLS coupling is described by the Hamiltonian

$$H_{q-\mathrm{TLS}} = -\frac{1}{2}\sigma_z \sum_n V^{(n)} \hat{\tau}_z^{(n)}. \tag{9}$$

Here $n = 1, \ldots, N_{\mathrm{TLS}}$ enumerates the TLSs, $\hat{\tau}_z^{(n)}$ is the Pauli operator of the nth TLS, and $V^{(n)}$ is the coupling parameter; the states of an nth TLS are $|0\rangle^{(n)}$ and $|1\rangle^{(n)}$, and $\hat{\tau}_z^{(n)}\,|i\rangle^{(n)} = (-1)^i\,|i\rangle^{(n)}$ with $i = 0, 1$. Hamiltonian $H_{q-\mathrm{TLS}}$ has the same form as the Hamiltonian of the qubit frequency fluctuations H_{fl} except that the fluctuations are described by operators in the TLSs' space. Such treatment is advantageous in view of formulation (3), as the qubit and TLSs are analyzed on an equal footing.

One needs to take into account the fact that the mean populations of the states of a TLS are different, generally. The difference is given by the expectation value $\langle\hat{\tau}_z^{(n)}\rangle$. It leads to a change of the mean qubit frequency compared to its value in the absence of the coupling to TLSs. However, it is the mean qubit frequency in the presence of the coupling that is observed in the experiment. Therefore, the operator of the qubit frequency noise can be defined as

$$\delta\hat{\omega}_q(t) = \sum_n V^{(n)}(\hat{\tau}_z^{(n)} - \langle\hat{\tau}_z^{(n)}\rangle), \tag{10}$$

in which case it has a zero-mean expectation value, $\langle\delta\hat{\omega}_q(t)\rangle = 0$.

An important characteristic of the qubit frequency noise is its power spectrum $S_q(\omega)$,

$$S_q(\omega) = \int_{-\infty}^{\infty} dt e^{i\omega t}\langle\delta\hat{\omega}_q(t)\delta\hat{\omega}_q(0)\rangle. \tag{11}$$

The expression for $S_q(\omega)$ follows from the dynamics of an isolated TLS being described by the standard Bloch equations if we disregard the backaction; see Sec. VII. The relevant parameters are the rates $W_{ij}^{(n)}$ of the interstate switching $|i\rangle^{(n)} \to |j\rangle^{(n)}$, where i and j take on values 0 and 1. From the balance equation for the state populations we have

$$\langle\hat{\tau}_z^{(n)}(t)\hat{\tau}_z^{(n)}(0)\rangle - \langle\hat{\tau}_z^{(n)}\rangle^2 = w^{(n)2}\exp(-W^{(n)}t), \tag{12}$$

where $W^{(n)}$ is the relaxation rate of the nth TLS. The parameters in this expression have the form

$$\begin{aligned} W^{(n)} &= W_{01}^{(n)} + W_{10}^{(n)}, \qquad \langle\hat{\tau}_z^{(n)}\rangle = \Delta W^{(n)}/W^{(n)}, \\ \Delta W^{(n)} &= W_{10}^{(n)} - W_{01}^{(n)}, \qquad w^{(n)} = 2(W_{01}^{(n)}W_{10}^{(n)})^{1/2}/W^{(n)}. \end{aligned} \tag{13}$$

From Eq. (12), the power spectrum of the qubit frequency noise is

$$S_q(\omega) = 2\sum_{n=1}^{N_{\mathrm{TLS}}} (w^{(n)}V^{(n)})^2 W^{(n)}/(W^{(n)2} + \omega^2). \tag{14}$$

This is the familiar form of the TLS-induced frequency noise as a sum of Lorentzians.

In the standard way, in what follows we call TLSs with equal switching rates $W_{01}^{(n)} = W_{10}^{(n)}$ symmetric, whereas those with unequal rates are called asymmetric. If the difference in the energy levels of a TLS exceeds k_BT, such a TLS is significantly asymmetric.

B. Explicit general expressions for the mean and correlator of measurement outcomes r_1 and $r_2(k)$

The effect of TLSs on the qubit dynamics depends on the relation between the couplings $V^{(n)}$ and $W_{ij}^{(n)}$. Our analysis gives the explicit expressions for the probability r_1 of having "1" as an outcome of the Ramsey measurement and for the pair correlation function $r_2(k)$, for an arbitrary ratio $V^{(n)}/W_{ij}^{(n)}$. In particular, we find that

$$r_1 = \frac{1}{2} + \frac{1}{2}e^{-t_R/T_2}\mathrm{Re}\left[e^{i\tilde{\phi}_R}\prod_n \Xi^{(n)}(t_R)\right], \tag{15}$$

where

$$\Xi^{(n)}(t_R) = \left[\left(\frac{W^{(n)}}{2\gamma^{(n)}} + iV^{(n)}\frac{\Delta W^{(n)}}{\gamma^{(n)}W^{(n)}}\right)\sinh\gamma^{(n)}t_R + \cosh\gamma^{(n)}t_R\right]\exp(-W^{(n)}t_R/2) \tag{16}$$

and

$$\tilde{\phi}_R = \left(\omega_q - \omega_{\mathrm{ref}} - \sum_n V^{(n)}\Delta W^{(n)}/W^{(n)}\right)t_R. \tag{17}$$

We emphasize that here ω_q is the observable qubit frequency as measured in the experiment. It refers to $\langle\delta\hat{\omega}_q\rangle = 0$.

The effect of TLSs on probability r_1 is described by factor $\Xi^{(n)}$. The expression for $\Xi^{(n)}$ coincides with the previously obtained expression for the factor that describes

the decay of $\langle\sigma_{\pm}(t)\rangle$ due to the coupling to TLSs [25]. The form of $\Xi^{(n)}$ is determined by parameter $\gamma^{(n)}$,

$$\gamma^{(n)} = \tfrac{1}{2}[W^{(n)2} + 4iV^{(n)}(\Delta W^{(n)} + iV^{(n)})]^{1/2}, \tag{18}$$

which depends on the interrelation between $V^{(n)}$ and the TLS relaxation rate $W^{(n)}$. It also depends on the TLS asymmetry $\Delta W^{(n)}$. Equation (15) shows that, as expected from the qualitative arguments, the TLS-induced change of the measurement probability is determined by the product of the contributions from individual TLSs.

We note that the expression for $\Xi^{(n)}(t_R)$ simplifies in the limit where the switching rate from one of the states of the nth TLS is zero, i.e., $W_{01}^{(n)}W_{10}^{(n)} = 0$ or, equivalently, $|\Delta W^{(n)}| = W^{(n)}$. In this limit $\Xi^{(n)}(t_R) = \exp[iV^{(n)}t_R\,\mathrm{sgn}(\Delta W^{(n)})]$. The corresponding TLS is not fluctuating; it stays in state $|0\rangle^{(n)}$ or $|1\rangle^{(n)}$ for $\Delta W^{(n)} > 0$ or $\Delta W^{(n)} < 0$, respectively. The coupling to such a TLS leads just to a static shift of the qubit frequency. A special analysis is required in the case of very small $W_{01}^{(n)}W_{10}^{(n)}/(W^{(n)})^2$, as one has to compare the total duration of the measurement sequence with the reciprocal minimal switching rate. In the present paper we assume that the total duration of the measurement sequence is much larger than $\max[(W_{ij}^{(n)})^{-1}]$.

The correlator of the measurement outcomes $r_2(k)$ due to the coupling to TLSs is described by a more complicated expression. As mentioned above, it should contain contributions from the decay of groups of different numbers of TLSs. The expression below shows that $r_2(k)$ for $k > 0$ is actually expressed in terms of a sum over such groups. The number of TLSs in each group is given by s, with $N_{\mathrm{TLS}} \geq s \geq 1$, where N_{TLS} is the total number of TLSs. A group with a given s includes all possible subsets $\{m\}_s = m_1, m_2, \ldots, m_s$, i.e., all possible combinations of s TLSs (m_i enumerates the TLSs within the group, $N_{\mathrm{TLS}} \geq m_i \geq 1$ for $i = 1, \ldots, s$). The centered correlator for $k > 0$ has the form

$$\tilde{r}_2(k) = \frac{1}{4}e^{-2t_R/T_2}\sum_{s=1}^{N_{\mathrm{TLS}}}\sum_{\{m\}_s}\left\{\mathrm{Re}\left(e^{i\tilde{\phi}_R}\left[\prod_{j=1}^{s}\xi_k^{(m_j)}(t_R)\right]\left[\prod_{n\notin\{m\}_s}\Xi^{(n)}(t_R)\right]\right)\right\}^2,$$
$$\xi_k^{(n)}(t_R) = iw^{(n)}(V^{(n)}/\gamma^{(n)})e^{-kW^{(n)}t_{\mathrm{cyc}}/2}\sinh\gamma^{(n)}t_R, \tag{19}$$

where $\Xi^{(n)}(t_R)$ and the characteristic coupling parameter $\gamma^{(n)}$ are given by Eqs. (16) and (18), respectively. The sum $\sum_{\{m\}_s}$ implies summation over all combinations of s TLSs, i.e., over all $m_1, m_2, \ldots, m_s$. The values of $m_1, \ldots, m_s$ can be arranged as $N_{\mathrm{TLS}} \geq m_1 > m_2 > \cdots > m_s \geq 1$. We note that the number of terms is exponential in the number N_{TLS} of TLSs.

The derivations of the above results based on the master equation for the coupled qubit and TLSs are given in Secs. VII and VIII. In Appendix A we provide an alternative derivation where the effect of TLSs is modeled by telegraph noise, i.e., $\delta\omega_q(t)$ in Eq. (1) is assumed to be telegraph noise.

Equation (19) provides an explicit solution of the problem of the correlation function of the measurement outcomes of a qubit coupled to TLSs $\tilde{r}_2(k)$. It holds for arbitrary ratios of the coupling parameters $|V^{(n)}|$ and the decay rates of TLSs $W^{(n)}$ and also for arbitrary ratios of these parameters to the reciprocal duration of the Ramsey measurement t_R^{-1}. The general expressions for r_1 and $\tilde{r}_2(k)$ simplify in the limiting cases of strong and weak coupling, i.e., large and small $|V^{(n)}|/W^{(n)}$ as well as in the case of comparatively small t_R. The corresponding limiting cases are discussed in the following subsections. For concreteness, we assume that $V^{(n)} > 0$, as the change in the sign of $V^{(n)}$ corresponds to swapping the TLS states $|0\rangle^{(n)}$ and $|1\rangle^{(n)}$.

C. Weak coupling

The weak coupling case, where $V^{(n)} \ll W^{(n)}$, is interesting not only on its own, but also because it extends to the case where noise of TLSs is Gaussian. The Gaussian limit corresponds to $V^{(n)} \propto N_{\mathrm{TLS}}^{-1/2}$ with the number of TLSs $N_{\mathrm{TLS}} \gg 1$ (the central limit theorem), but we emphasize that the expressions in this subsection are not based on the assumption of Gaussianity. We start with a formal expansion of the general expressions for r_1 and $r_2(k)$ and then provide a physical insight into the results.

Formally, for $V^{(n)} \ll W^{(n)}$, we can expand parameter $\gamma^{(n)}$ in Eq. (18) to second order in $V^{(n)}/W^{(n)}$. Substituting the expansion into expression (15) for the probability r_1 of having "1" as the Ramsey measurement outcome, we obtain

$$r_1 \approx \frac{1}{2} + \frac{1}{2}\exp\left(-\frac{t_R}{T_2} - \frac{1}{2}\langle\hat{\theta}^2\rangle\right)\cos\phi_R,$$
$$\langle\hat{\theta}^2\rangle = \sum_n 2(w^{(n)}V^{(n)}/W^{(n)})^2(W^{(n)}t_R + e^{-W^{(n)}t_R} - 1). \tag{20}$$

Here ϕ_R is the control phase defined by Eq. (8). Equation (20) applies for both symmetric and asymmetric TLSs.

The term $\langle\hat{\theta}^2\rangle$ in Eq. (20) is the expectation value of the variance of the random phase of the qubit

$$\hat{\theta}_k = \sum_{n=1}^{N_{\rm TLS}} \hat{\theta}_k^{(n)} = \int_{kt_{\rm cyc}}^{kt_{\rm cyc}+t_R} dt\, \delta\hat{\omega}_q(t) \tag{21}$$

accumulated over time t_R during the kth Ramsey measurement. From Hamiltonian (9), contribution $\hat{\theta}_k^{(n)}$ of an nth TLS to this phase is

$$\hat{\theta}_k^{(n)} = V^{(n)} \int_{kt_{\rm cyc}}^{kt_{\rm cyc}+t_R} dt[\hat{\tau}_z^{(n)}(t) - \langle\hat{\tau}_z^{(n)}\rangle]. \tag{22}$$

For independent TLSs, the variance of phase $\hat{\theta}_k$ is a sum of the variances of the "partial" phases $\hat{\theta}_k^{(n)}$. Clearly, $\langle\theta_k^{(n)2}\rangle$ is independent of the cycle number k. Equation (20) follows from the expression for $\langle\theta^{(n)2}\rangle$ obtained from Eq. (12).

For small $W^{(n)}t_R$, we have

$$\langle\hat{\theta}^2\rangle \approx \sum_n (w^{(n)}V^{(n)}t_R)^2, \qquad W^{(n)}t_R \ll 1. \tag{23}$$

It is seen from Eq. (20) that in this case $r_1 - 1/2$ displays a Gaussian decay with t_R, i.e., $\log(r_1 - 1/2) \propto -t_R^2$ for $t_R \ll T_2$; no assumption about the TLS spectrum is needed. On the other hand, for longer Ramsey times or faster switching TLSs, $W^{(n)}t_R > 1$, the decay of $r_1 - 1/2$ with increasing t_R is close to exponential.

In the weak-coupling limit, to leading order in $V^{(n)}/W^{(n)}$, Eq. (19) for the centered pair correlator $\tilde{r}_2(k)$ can be put in the form that relates it to the correlator of the overall qubit phase $\hat{\theta}_k$,

$$\tilde{r}_2(k) \approx \tfrac{1}{4}e^{-2t_R/T_2 - \langle\hat{\theta}^2\rangle} \sin^2\phi_R \langle\hat{\theta}_0\hat{\theta}_k\rangle. \tag{24}$$

Since the TLSs are uncorrelated, the correlator of phase $\hat{\theta}$ is given by the sum of the correlators of the phases of individual TLSs

$$\begin{aligned}\langle\hat{\theta}_0\hat{\theta}_k\rangle &= \sum_n \langle\hat{\theta}_0^{(n)}\hat{\theta}_k^{(n)}\rangle,\\ \langle\hat{\theta}_0^{(n)}\hat{\theta}_k^{(n)}\rangle &= (2V^{(n)}w^{(n)}/W^{(n)})^2\\ &\quad\times \exp(-kW^{(n)}t_{\rm cyc})\sinh^2(W^{(n)}t_R/2), \qquad k \geq 1.\end{aligned} \tag{25}$$

Equation (25) follows from Eqs. (22) and (12). Importantly, the correlator of phase $\hat{\theta}$ is directly expressed in terms of the power spectrum $S_q(\omega)$ of the TLS-induced frequency noise (11),

$$\langle\hat{\theta}_0\hat{\theta}_k\rangle = \frac{1}{\pi}\int d\omega e^{ik\omega t_{\rm cyc}} S_q(\omega)(1-\cos\omega t_R)/\omega^2. \tag{26}$$

We note that in this expression, along with the standard factor $(1-\cos\omega t_R)/\omega^2$, the spectrum $S_q(\omega)$ is weighted with the factor $\exp(ik\omega t_{\rm cyc})$. To find correlator $\langle\hat{\theta}_0\hat{\theta}_k\rangle$ for large $kt_{\rm cyc}/t_R$, one can often set $(1-\cos\omega t_R)/\omega^2 \approx t_R^2/2$; see below.

Equation (24) gives the correlator of the measurement outcomes $\tilde{r}_2(k)$ in a simple explicit form for weak coupling, i.e., in the case where the partial contributions of different TLSs to the random qubit phase $\langle\hat{\theta}^{(n)2}\rangle$ are small on average. A partial contribution of an nth TLS to $\tilde{r}_2(k)$, which is proportional to $\langle\hat{\theta}_0^{(n)}\hat{\theta}_k^{(n)}\rangle$, is quadratic in the ratio $V^{(n)}/W^{(n)}$. Since each such contribution decays with k as $\exp(-kW^{(n)}t_{\rm cyc})$, the overall decay of $\tilde{r}_2(k)$ with k is nonexponential. It is important that the expression for $\tilde{r}_2(k)$ contains the factor $\exp(-\langle\hat{\theta}^2\rangle)$ that describes the collective effect of the system of TLSs on the contribution of an individual TLS to the decay. Even though, for weak coupling, $\langle\hat{\theta}^{(n)2}\rangle \ll 1$ for each TLS, $\langle\hat{\theta}^2\rangle = \sum_n\langle\hat{\theta}^{(n)2}\rangle$ does not have to be small, if the number of TLSs is large.

D. Short Ramsey accumulation time

The general expressions (15) and (19) for probability r_1 and the centered pair correlator $\tilde{r}_2(k)$ are also simplified in the case where the Ramsey wait (accumulation) time is short or the coupling is weak and the switching rates are small, so that $V^{(n)}t_R, W^{(n)}t_R \ll 1$. In this case functions $\Xi^{(n)}$ and $\xi_k^{(n)}$ in Eqs. (15) and (19) take the form

$$\begin{aligned}\Xi^{(n)}(t_R) &\approx \exp[i(\Delta W^{(n)}/W^{(n)})V^{(n)}t_R - (w^{(n)}V^{(n)}t_R)^2/2],\\ \xi_k^{(n)}(t_R) &\approx iw^{(n)}V^{(n)}t_R\exp(-kW^{(n)}t_{\rm cyc}).\end{aligned} \tag{27}$$

This gives, to leading order in the small parameters,

$$r_1 \approx \frac{1}{2} + \frac{1}{2}\exp\left[-t_R/T_2 - \sum_n (w^{(n)}V^{(n)}t_R)^2/2\right]\cos\phi_R \tag{28}$$

and

$$\begin{aligned}\tilde{r}_2(k) \approx \frac{1}{4}e^{-2t_R/T_2}\sum_n \sin^2(\phi_R - V^{(n)}\Delta W^{(n)}t_R/W^{(n)})\\ \times (w^{(n)}V^{(n)}t_R)^2 e^{-kW^{(n)}t_{\rm cyc}}.\end{aligned} \tag{29}$$

Equations (28) and (29) hold for arbitrary ratios $V^{(n)}/W^{(n)}$. The considered limit is physically important. Indeed, TLSs with $W^{(n)}t_R \gg 1$ do not contribute to the centered correlators $\tilde{r}_2(k)$ and higher-order centered correlators: fast

switching averages out their effect. Correlators $\tilde{r}_2(k)$ are formed mainly by TLSs with switching rates smaller than $t_{\rm cyc}^{-1} < t_R^{-1}$, i.e., $W^{(n)}t_R < 1$.

The condition $V^{(n)}t_R \ll 1$ is another condition of an effectively weak coupling. It is different from that discussed in Sec. III C. It shows that the coupling to an nth TLS weakly affects the phase accumulated by the qubit during the Ramsey measurement. The effect of this coupling on r_1 and $\tilde{r}_2(k)$ can thus be described by keeping the lowest-order terms in $V^{(n)}$. This leads to simple explicit expressions for r_1 and $\tilde{r}_2(k)$, Eqs. (28) and (29). As in the case of small $|V^{(n)}|/W^{(n)}$, the decay of $\tilde{r}_2(k)$ is described by the sum of exponential factors $\exp(-kW^{(n)}t_{\rm cyc})$ that come from individual TLSs. However, now each of these factors is weighted with the coefficient $\propto (V^{(n)}t_R)^2$.

Equations (28) and (29) deserve comments. From Eq. (28), r_1 as a function of ϕ_R is maximal for $\phi_R = 0$. Since ϕ_R is determined by the difference between the qubit frequency and the frequency of the reference drive, it means that the qubit frequency is equal to the reference frequency when r_1 is maximal even in the presence of coupling to asymmetric TLSs.

From Eq. (29), correlator $\tilde{r}_2(k)$ goes to zero to second order in $V^{(n)}t_R$ for $\phi_R = 0$. In fact, in region $|\phi_R| \lesssim |V^{(n)}|t_R$ one has to allow for higher-order terms in $V^{(n)}t_R$ in the expression for $\tilde{r}_2(k)$. We give this expression for the case of symmetric TLSs, where $\Delta W^{(n)} = 0$. Here, for $N_{\rm TLS} \geq 2$, for small $|\phi_R|$, and to leading order in $V^{(n)}t_R, W^{(n)}t_R$, one has to add an extra term $\delta\tilde{r}_2(k)$ to expression (29) for $\tilde{r}_2(k)$,

$$\delta\tilde{r}_2(k) \approx \frac{1}{4}e^{-2t_R/T_2}\sum_{m_1=2}^{N_{\rm TLS}}\sum_{m_2=1}^{m_1-1}(V^{(m_1)}V^{(m_2)}t_R^2)^2 \times \exp[-k(W^{(m_1)} + W^{(m_2)})t_{\rm cyc}]. \quad (30)$$

Equations (29) and (30) show that not only is $\tilde{r}_2(k)$ small for small ϕ_R, but $\tilde{r}_2(k)$ falls off much faster with increasing k for $\phi_R = 0$ than for $\phi_R = \mathcal{O}(1)$. This feature allows one to identify the frequency noise as being due to the coupling to TLSs.

E. Centered three-time correlator $\tilde{r}_3$ for weak coupling

It follows from Eq. (7) [see also Eq. (37) below and Sec. IX] that, to leading order in the coupling to TLSs, the three-time correlator of the measurement outcomes is expressed in terms of the three-time correlator of the qubit phase,

$$\begin{aligned}\tilde{r}_3(k,\ell) &= \langle[p(\theta_0) - \langle p(\theta)\rangle][p(\theta_k) \\ &\quad - \langle p(\theta)\rangle][p(\theta_\ell) - \langle p(\theta)\rangle]\rangle \\ &\approx -\tfrac{1}{8}e^{-3t_R/T_2}\langle\hat{\theta}_0\hat{\theta}_k\hat{\theta}_\ell\rangle\sin^3\phi_R. \end{aligned} \quad (31)$$

A straightforward calculation using the approach of Sec. VII shows that

$$\langle\hat{\theta}_0\hat{\theta}_k\hat{\theta}_\ell\rangle \approx -\sum_n (2V^{(n)}/W^{(n)})^3 w^{(n)2}\Delta W^{(n)}t_R \times \exp(-\ell W^{(n)}t_{\rm cyc})\sinh^2(W^{(n)}t_R/2) \quad (32)$$

for $\ell > k > 0$.

Equation (32) shows that, to leading order in the coupling parameters $V^{(n)}$, only asymmetric TLSs, for which $\Delta W^{(n)}$ is nonzero, contribute to $\tilde{r}_3$. It should be noted that the value of $\tilde{r}_3$ is maximal for $\phi_R = \pi/2$. This will be used in the analysis below. Somewhat unexpectedly, the dependence of $\tilde{r}_3(k,\ell)$ on k and ℓ is given by the sum of the appropriately weighted factors $\exp(-\ell W^{(n)}t_{\rm cyc})$, i.e., $\tilde{r}_3(k,\ell)$ is independent of k. We note that, to higher order in the coupling, $\tilde{r}_3$ has contributions from symmetric TLSs as well.

F. Strong coupling

In the limit of strong coupling to TLSs, $V^{(n)} \gg W^{(n)}$, to leading order

$$r_1 \approx \frac{1}{2} + \frac{1}{2}e^{-t_R/T_2}\mathrm{Re}\left\{e^{i\tilde{\phi}_R}\prod_n e^{-W^{(n)}t_R/2} \times [\cos V^{(n)}t_R + i(\Delta W^{(n)}/W^{(n)})\sin V^{(n)}t_R]\right\} \quad (33)$$

(for brevity, this expression is provided for the case $\Delta W^{(n)}t_R \ll 1$).

The dependence of r_1 on the duration of the Ramsey measurement t_R is determined by the product of the oscillating factors. For $V^{(n)}t_R \ll 1$, we have $r_1 - 1/2 \propto \exp(-\sum_n V^{(n)2}t_R^2/2)$. As the characteristic $V^{(n)}t_R$ increases, $r_1 - 1/2$ quickly falls off for a large number of TLSs if the values of $V^{(n)}$ are broadly distributed.

The behavior becomes more complicated in the range where $V^{(n)}t_R$ is not small and the values of $V^{(n)}$ for different TLSs are close to each other. This is a consequence of the oscillating factor in Eq. (33). For symmetric TLSs ($\Delta W^{(n)} = 0$), we have $r_1 - 1/2 \propto (\cos V^{(n)}t_R)^{N_{\rm TLS}}$, which is a sharp periodic function of $V^{(n)}t_R$ for a large number of TLSs. The nonmonotonic dependence of $r_1 - 1/2$ on t_R is a specific effect that allows one to reveal the presence of TLSs with close values of the coupling to a qubit.

Strong coupling to a qubit is most pronounced if $V^{(n)}t_R \gtrsim 1$, while at the same time $t_R \ll T_2$. It is plausible that only one TLS meets this condition along with the condition $V \gg W$, where V and W are the coupling parameter and the switching rate of this TLS. In this case r_1 oscillates with t_R with period $2\pi/V$; cf. Ref. [54]. Importantly, correlator $\tilde{r}_2(k)$ is oscillating with half of this period. For a

symmetric TLS,

$$\tilde{r}_2(k) \approx \tfrac{1}{4} e^{-2t_R/T_2} \sin^2\phi_R \sin^2(Vt_R) \exp(-kWt_{\rm cyc}). \quad (34)$$

The combination of the oscillations of the expectation value r_1 with respect to t_R with period $2\pi/V$ and of correlator $\tilde{r}_2(k)$ with period π/V is a distinctive feature of a strong dispersive coupling to a single TLS. It allows one to fairly unambiguously identify the strong coupling to a single TLS as the decoherence mechanism. We note that, in superconductor-based systems of qubits, one of the qubits can serve as a TLS that causes dephasing of another qubit. One can also see from the comparison of Eq. (34) with Eq. (38) below that the dependence of $\tilde{r}_2(k)$ on the angle ϕ_R is different for a TLS and for Gaussian frequency noise, if the coupling is not weak.

IV. GAUSSIAN FLUCTUATIONS OF THE QUBIT FREQUENCY

An important cause of the qubit frequency fluctuations is external classical noise with frequencies much lower than the qubit transition frequency. The effect of such noise is described by the term $-\frac{1}{2}\delta\omega_q(t)\sigma_z$ in the qubit Hamiltonian; cf. Eq. (1). We consider zero-mean stationary Gaussian frequency fluctuations $\delta\omega_q(t)$. Such fluctuations are fully characterized by their power spectrum

$$S_q(\omega) = \int_{-\infty}^{\infty} dt e^{i\omega t} \langle \delta\omega_q(t)\delta\omega_q(0)\rangle. \quad (35)$$

This expression has the same form as Eq. (11) for the TLS-induced frequency noise, except that $\delta\omega_q(t)$ is not an operator. For classical fluctuations, $S_q(\omega) = S_q(-\omega)$. The technique we develop can be extended to quantum noise as well.

A. Explicit general expressions

Of relevance for the qubit is the accumulation of its phase due to frequency fluctuations. For a classical noise of the qubit frequency, the phase accumulated over the time interval $(kt_{\rm cyc}, kt_{\rm cyc} + t_R)$, i.e., during the kth Ramsey measurement, is $\theta_k = \int_{kt_{\rm cyc}}^{kt_{\rm cyc}+t_R} \delta\omega_q(t)dt$; cf. Eq. (2). This expression is the classical analog of operator $\hat{\theta}_k$.

The correlation function f_k of phases accumulated during measurements separated by k cycles,

$$f_k \equiv \langle \theta_n \theta_{n+k}\rangle, \quad (36)$$

is related to the noise power spectrum $S_q(\omega)$ by Eq. (26). Here we use the fact that, because of the stationarity of noise $\delta\omega_q(t)$, correlator $\langle\theta_n\theta_m\rangle$ depends only on $|n-m|$. The probability distribution of phases θ_n is Gaussian for the Gaussian distribution of $\delta\omega_q(t)$. It is thus fully determined by parameters f_k. As seen from Eqs. (36) and (26), $f_0 > 0$ and $f_0 \geq |f_k|$ for $k \neq 0$. While $f_k = f_{-k}$, correlators f_k can be negative, in general.

The phase correlators are directly related to probability r_1 and correlators $r_2(k), r_3(k,\ell)$ of the Ramsey measurements. Intuitively, one can express these parameters in terms of the probability $p(\theta)$, Eq. (7), of having "1" as an outcome of the Ramsey measurement for a given θ,

$$r_1 = \langle p(\theta_n)\rangle, \qquad r_2(k) = \langle p(\theta_n)p(\theta_{n+k})\rangle,$$
$$r_3(k,\ell) = \langle p(\theta_n)p(\theta_{n+k})p(\theta_{n+\ell})\rangle. \quad (37)$$

The averaging here is done over the distribution of phases $\{\theta\}$. For the stationary distribution, the result is independent of n.

Equation (37) applies independent of the noise statistics. It is substantiated by the analysis of Sec. IX, which is based on solving the master equation for a qubit in the presence of noise. For Gaussian noise, we have, for $l > k > 0$,

$$r_1 = \tfrac{1}{2}[1 + e^{-t_R/T_2}\exp(-f_0/2)\cos\phi_R],$$
$$\tilde{r}_2(k) = \tfrac{1}{8} e^{-2t_R/T_2}\exp(-f_0)[e^{f_k} - 1 - \cos(2\phi_R)(1 - e^{-f_k})], \quad (38)$$

and

$$\tilde{r}_3(k,\ell) = \frac{1}{32}\exp[-3(f_0/2) - 3(t_R/T_2)]\Big\{\cos 3\phi_R\Big[\exp\Big(-\sum_i f_i\Big) + 2 - \sum_i \exp(-f_i)\Big]$$
$$+ \cos\phi_R\Big[\sum_i \exp\Big(-f_i + \sum_j{}' f_j\Big) + 6 - \sum_i (2e^{f_i} + e^{-f_i})\Big]\Big\}. \quad (39)$$

In Eq. (39) the sums over i,j run over $i,j = k,l,l-k$, and the prime over the sum means that $j \neq i$.

For weak noise, $f_k \ll 1$, the centered pair and triple correlators are

$$\tilde{r}_2(k) \approx \tfrac{1}{4} e^{-2t_R/T_2}\exp(-f_0) f_k \sin^2\phi_R, \tilde{r}_3(k,\ell) \approx -\tfrac{1}{8} e^{-3t_R/T_2}\exp(-3f_0/2)(f_k f_\ell + f_k f_{\ell-k} + f_\ell f_{\ell-k})\cos\phi_R \sin^2\phi_R. \quad (40)$$

We keep the term $\propto f_0$ in the exponent to account for the case where parameters $f_{n>0}$ are small because the period of the measurements largely exceeds the correlation time of the noise, $t_{\rm cyc} \gg \tau_{\rm corr}$. Correlator $\tilde{r}_2(k)$ is of first order in f_k whereas correlator $\tilde{r}_3(k,\ell)$ is bilinear in f_k, f_ℓ.

In the opposite limit of strong noise, where $\exp(-f_0) \ll 1$, r_1 approaches 1/2. However, the pair correlator $r_2(k)$ does not necessarily become small for not too large k, if the noise is strongly correlated, $\tau_{\rm corr} \gg t_{\rm cyc}$. Indeed, in this case one may have $f_0 - f_k \ll 1$, so that $\tilde{r}_2(k) \approx \frac{1}{8}\exp(f_k - f_0)$ for $t_R \ll T_2$. This is an interesting and unexpected feature of the noise with a long correlation time. It enables revealing such characteristic noise correlations through periodically repeated measurements. We note that, in contrast to $\tilde{r}_2(k)$, quite generally, the triple correlator becomes small, $\tilde{r}_3(k,\ell) \propto (r_1 - 1/2)$, which is another characteristic feature of the noise.

B. Differentiating Gaussian from non-Gaussian noise

Not only does correlator $\tilde{r}_3(k,\ell)$ directly provide important information about the qubit frequency noise, but it also allows one to distinguish Gaussian and non-Gaussian noise. Generally, as seen from Eq. (38), for Gaussian noise, correlators f_k can be found for all k by measuring r_1 and $\tilde{r}_2(k)$. They then define $\tilde{r}_3(k,\ell)$. Therefore, by measuring $\tilde{r}_3(k,\ell)$ using the same data array, and by comparing with what is expected from the measured r_1 and $\tilde{r}_2(k)$ one can tell whether the frequency noise is non-Gaussian.

There are also additional signs of Gaussianity versus non-Gaussianity. In particular, for Gaussian noise, $r_1 > 1/2$. By construction, matrix $F_{n\,n+k} \equiv \langle\theta_n\theta_{n+k}\rangle$ is symmetric and positive definite, $F_{n\,n+k} \equiv f_k$. It also follows from Eq. (39) that, for Gaussian noise, the centered correlator $\tilde{r}_3$ goes to zero as ϕ_R approaches $\pi/2$. This is another prerequisite of Gaussianity. At the same time, for weak Gaussian noise, where $f_k \ll 1$, we have, from Eq. (38), $\tilde{r}_2(k) \propto f_k \sin^2\phi_R$, which means that in this limit $\tilde{r}_2 \to 0$ for $\phi_R \to 0$. Therefore one may be interested in measuring the pair and triple correlators for different values of ϕ_R and comparing the results.

Overall, for Gaussian noise, the correlators display a characteristic dependence on ϕ_R, as seen from the general expressions (38) and (39). While $\tilde{r}_2(k)$ contains a term that varies as $\cos(2\phi_R)$, the expression for $\tilde{r}_3(k,\ell)$ contain $\cos\phi_R$ and $\cos(3\phi_R)$. So, changing $\phi_R \to \pi - \phi_R$ does not change $\tilde{r}_2(k)$, but changes the sign of $\tilde{r}_3(k,\ell)$ for Gaussian noise. The above features provide a straightforward means for establishing whether the low-frequency qubit noise is Gaussian.

C. Exponentially correlated frequency noise

We now provide explicit expressions for correlators $f_k = \langle\theta_n\theta_{n+k}\rangle$ of phases accumulated during a Ramsey measurement for three explicit types of Gaussian frequency noise. The results for the two most frequently used models are compared in Sec. VI C with simulations. The effect of noise correlations comes into play if the characteristic correlation time is comparable to $t_{\rm cyc}$. Otherwise, one can think of frequency noise as white (δ correlated). For $\langle\delta\omega_q(t)\delta\omega_q(t')\rangle = D_w\delta(t-t')$, we have

$$f_k = D_w t_R \delta_{k,0},$$

where D_w is white noise intensity. For such noise, the centered measurement correlators $\tilde{r}_2(k), \tilde{r}_3(k,\ell)$ should vanish, as indeed seen from Eqs. (38) and (39).

An important type of correlated Gaussian noise is exponentially correlated noise (the Ornstein-Uhlenbeck process),

$$\langle\delta\omega_q(t)\delta\omega_q(t')\rangle = \tfrac{1}{2}D_{\rm corr}\tau_{\rm corr}^{-1}e^{-|t-t'|/\tau_{\rm corr}}. \tag{41}$$

The power spectrum of such noise is Lorentzian,

$$\begin{aligned} S_q(\omega) &\equiv \int_{-\infty}^{\infty} dt e^{i\omega t}\langle\delta\omega_q(t)\delta\omega_q(0)\rangle \\ &= D_{\rm corr}/(1+\omega^2\tau_{\rm cor}^2). \end{aligned} \tag{42}$$

Quite often the expression "colored noise" is used for the noise with spectrum (42). However, this is, of course, not the only noise spectrum that differs from the flat spectrum of white noise, and therefore we use the more specific term "exponentially correlated noise."

Exponentially correlated noise may come from a filtered white Gaussian noise, a simple example being broadband random voltage filtered by an *RC* circuit. Another example is noise from dispersive coupling to thermal photons in a multimode cavity with the mode decay times being close to each other, so that these times can be approximated by $\tau_{\rm corr}$. Such noise was also used to model the effect of coupling of an electron spin to a bath of nuclear spins [55]. In Eq. (41) $D_{\rm corr}$ characterizes noise intensity, whereas $\tau_{\rm corr}$ is the noise correlation time.

Using Eq. (36), which expresses the phase correlators f_k in terms of the power spectrum $S_q(\omega)$, one obtains

$$\begin{aligned} f_0 &= D_{\rm corr}[t_R - \tau_{\rm corr}(1 - e^{-t_R/\tau_{\rm corr}})], \\ f_k &= D_{\rm corr}\tau_{\rm corr}\exp(-|k|t_{\rm cyc}/\tau_{\rm corr}) \\ &\quad \times [\cosh(t_R/\tau_{\rm corr}) - 1], \qquad |k| > 0. \end{aligned} \tag{43}$$

As seen from Eq. (43), correlators f_k fall off exponentially with increasing $|k|$ for exponentially correlated noise. The rate of the decay is determined by the relation between the duration of cycle $t_{\rm cyc}$ and the noise correlation time $\tau_{\rm corr}$.

From Eq. (40), for weak noise, $f_n \ll 1$, correlator $\tilde{r}_2(k)$ falls off exponentially with increasing k. Correlator $\tilde{r}_3(k,\ell)$, on the other hand, which is quadratic in f_n,

shows nonexponential decay even where the decay of $\tilde{r}_2(k)$ is close to exponential. This is in agreement with the simulations discussed in Sec. VI C.

It is important that, for stronger noise, the decay of correlators $\tilde{r}_2(k), \tilde{r}_3(k,\ell)$ becomes nonexponential, even though f_k exponentially falls off with increasing k.

D. Noise with "profound color"

To illustrate the possibility of a nonmonotonic behavior of correlators f_k as functions of k, we briefly describe the effect of noise with "profound color," that is, noise with a spectrum $S_q(\omega)$ that has a pronounced peak at a nonzero frequency. A simple example is Johnson-Nyquist noise filtered by an *RCL* circuit. The power spectrum of such noise is

$$S_q(\omega) = D_{\rm clr}[(\omega^2 - \omega_{\rm clr}^2)^2 + 4\Gamma_{\rm clr}^2\omega^2]^{-1}. \tag{44}$$

This spectrum has a peak at $(\omega_{\rm clr}^2 + 2\Gamma_{\rm clr}^2)^{1/2}$. For $\omega_{\rm clr} \gg \Gamma_{\rm clr}$, this peak is Lorentzian with halfwidth $\Gamma_{\rm clr}$.

It is straightforward to see that, for $\sqrt{2}\Gamma_{\rm clr}t_R < \omega_{\rm clr}t_R \ll 1$, we have

$$\begin{aligned} f_0 &= D_{\rm clr}t_R^2/4\omega_{\rm clr}^3 \sin\phi_{\rm clr}, \\ f_k &= \frac{D_{\rm clr}t_R^2}{2\omega_{\rm clr}^3 \sin(2\phi_{\rm clr})} \exp(-kt_{\rm cyc}\omega_{\rm clr}\sin\phi_{\rm clr}) \\ &\quad \times \cos(kt_{\rm cyc}\omega_{\rm clr}\cos\phi_{\rm clr} - \phi_{\rm clr}), \qquad k > 0, \end{aligned} \tag{45}$$

where

$$\phi_{\rm clr} = \frac{1}{2}\arctan\frac{2\Gamma_{\rm clr}\sqrt{\omega_{\rm clr}^2 - \Gamma_{\rm clr}^2}}{\omega_{\rm clr}^2 - 2\Gamma_{\rm clr}^2}.$$

From Eq. (45), correlators f_k display exponentially decaying oscillations as functions of k. For weak noise, such oscillations will be immediately seen in correlators $\tilde{r}_2(k)$. Other features of the effect of this noise will be discussed in a separate paper; here our goal is just to indicate that such noise may have an important effect on the qubit dynamics.

E. $1/f$ noise

Very often qubit decoherence is caused by $1/f$ frequency noise, i.e., by noise with the power spectrum $S_q(\omega) \propto 1/\omega \equiv 1/2\pi f$; cf. Refs. [5,14,29,39] and the references therein. If such noise comes from a large number of fluctuators, it becomes Gaussian, and the assumption that $1/f$ noise is Gaussian is often made. Since the integral intensity of $1/f$ noise diverges, the spectrum has to be cut both at low and high frequencies. A high-frequency cutoff is irrelevant for the problem of the qubit frequency noise that we consider, since the integration over interval t_R between the Ramsey pulses filters out high-frequency noise components.

The low-frequency cutoff is model dependent. We present results for a simple physically motivated model in which the spectrum is smooth. This model is also related to the model of noise from TLSs used in the simulations. In contrast to the simulated TLS models, it corresponds to coupling to a very large number of TLSs with the coupling constant being the same for all TLSs (cf. Refs. [8,56]) and with log-uniform distribution of the switching rates $W^{(n)}$; the rates are assumed to be limited from below by $\omega_{\rm min}$. From Eq. (12), the power spectrum of such noise has the form

$$\begin{aligned} S_q(\omega) &= \frac{2}{\pi}D_{\rm fl}\int_{\omega_{\rm min}}^{\infty}\frac{dW}{W^2+\omega^2} \\ &= D_{\rm fl}|\omega|^{-1}[1 - (2/\pi)\arctan|\omega_{\rm min}/\omega|]. \end{aligned} \tag{46}$$

In the range $\omega \gg \omega_{\rm min}$ we have $S_q(\omega) \approx D_{\rm fl}/\omega$, whereas $S_q(\omega) \approx 2D_{\rm fl}/\pi\omega_{\rm min}$ for $|\omega| \ll \omega_{\rm min}$.

Calculating the integral in Eq. (36) by closing the contour in the ω plane and using Eq. (46), one can write the correlators of the qubit phase accumulated during measurements separated by $kt_{\rm cyc}$ as

$$\begin{aligned} f_k &= \frac{2}{\pi}D_{\rm fl}\int_{\omega_{\rm min}}^{\infty}\frac{dW}{W^3}[\cosh(Wt_R) - 1] \\ &\quad \times \exp(-kWt_{\rm cyc}), \qquad k > 0, \end{aligned} \tag{47}$$

whereas the mean square phase $\langle\theta^2\rangle$ acquired by the qubit over time t_R is

$$f_0 = \frac{2}{\pi}D_{\rm fl}\left[\frac{t_R}{\omega_{\rm min}} + \int_{\omega_{\rm min}}^{\infty}\frac{dW}{W^3}(e^{-Wt_R} - 1)\right]. \tag{48}$$

For small $\omega_{\rm min}t_R \ll 1$, the leading-order terms in f_k and f_0 are logarithmic in $\omega_{\rm min}t_R$. The decay of correlators f_k with increasing k is nonexponential, in contrast to the case of exponentially correlated Gaussian noise. However, it gets close to exponential in the limit of large $k\omega_{\rm min}t_{\rm cyc} \gg 1$,

$$f_k \approx D_{\rm fl}(t_R^2/\pi kt_{\rm cyc}\omega_{\rm min})\exp(-k\omega_{\rm min}t_{\rm cyc}).$$

On the other hand, for $kt_{\rm cyc} \gg t_R$ but $k\omega_{\rm min}t_{\rm cyc} \ll 1$, a reasonable numerical approximation is

$$f_k \approx D_{\rm fl}(t_R^2/\pi)[-\gamma_E - \log(k\omega_{\rm min}t_{\rm cyc})], \tag{49}$$

where $\gamma_E \approx 0.58$ is the Euler constant.

The integrals in Eqs. (47) and (48) can be expressed in terms of exponential integral and hyperbolic integral functions. These expressions are given in Appendix C.

The explicit forms of correlators $\tilde{r}_2(k)$ and $\tilde{r}_3(k,\ell)$ for $1/f$ noise are discussed in Sec. VI C. The results show, in particular, the sensitivity of these correlators to the low-frequency threshold $\omega_{\rm min}$.

V. POWER SPECTRUM FOR WEAK FREQUENCY NOISE

In this section we study the relation between the power spectrum of the qubit frequency noise and the spectrum of the measurement outcomes. The power spectrum of N measurement outcomes is given by the discrete Fourier transform of the first N values of the pair correlator $\tilde{r}_2(k)$,

$$R(m) = 2\mathrm{Re}\sum_{k=0}^{N-1}\tilde{r}_2(k)e^{-2\pi imk/N}. \tag{50}$$

Here we defined, by continuity, $\tilde{r}_2(0) \equiv \langle (x_n - \langle x_n\rangle)^2\rangle = r_1(1-r_1)$.

One can similarly define a complex discrete bispectrum of the measurement outcomes as

$$R_{\mathrm{bispctr}}(m_1,m_2) = \sum_{k_1,k_2=0}^{N-1}\tilde{r}_3(k_1,k_2)e^{-2\pi i(m_1k_1+m_2k_2)/N},$$

where one sets $\tilde{r}_3(0,k) = \tilde{r}_3(k,0) = \langle (x_{n+k}-r_1)(x_n - r_1)^2\rangle$ and $\tilde{r}_3(k,k) = \langle (x_{n+k}-r_1)^2(x_n-r_1)\rangle$ for $k \geq 0$.

Spectrum $R(m)$ is immediately related to the directly evaluated discrete Fourier transform $X(m)$ of the measurement outcomes x_n,

$$X(m) = N^{-1/2}\sum_{n=0}^{N-1}x_n\exp(2\pi imn/N), \tag{51}$$

where x_n takes on the value 0 or 1. Taking into account the fact that, in the limit of large N, the centered correlator $\tilde{r}_2(k)$ decays already for $k \ll N$, we obtain a standard relation

$$\mathbb{E}[|X(m)|^2] = R(m) - r_1(1-r_1) + Nr_1^2\delta_{m,0}. \tag{52}$$

This relation allows one to compare the analytical results on $R(m)$ that follow from the explicit expressions for $\tilde{r}_2(k)$ with simulations of the spectrum.

Similarly, bispectrum $R_{\mathrm{bispectr}}(m_1,m_2)$ is related to $\mathbb{E}[X(m_1)X(m_2)X^*(m_1+m_2)]$.

For a weak qubit frequency noise $\delta\omega_q(t)$, the expression for the centered correlator $\tilde{r}_2(k)$, both for noise from TLSs and for Gaussian noise, can be written as

$$\tilde{r}_2(k) = \left(r_1 - \frac{1}{2}\right)^2\langle\theta_0\theta_k\rangle\tan^2\phi_R; \tag{53}$$

cf. Eqs. (24) and (40). As noted above, in the case of noise from TLSs one should use here $\langle\hat{\theta}_0\hat{\theta}_k\rangle$, i.e., the correlator of the random part of the phase accumulation, $\langle\hat{\theta}_m\rangle = 0$.

Equations (50) and (53) allow one to relate spectrum $R(m)$, and thus $\mathbb{E}[|X(m)|^2]$, to the power spectrum of qubit frequency noise $S_q(\omega)$ for weak noise. As seen from Eqs. (26) and (35), the dependence of $\langle\theta_0\theta_k\rangle$ on k is determined by factor $\exp(ik\omega t_{\mathrm{cyc}})$ weighted with $S_q(\omega)$ in the integral over ω. Therefore, summation over k in Eq. (50) can be easily done for $N\to\infty$. One then takes into account the fact that, for a real α, $\sin(N\alpha)/[1-\exp(i\alpha)] \to \pi\sum_\ell\delta(\alpha+2\pi\ell)$ (of interest to us is $\alpha = \omega t_{\mathrm{cyc}} - 2\pi m/N$), whereas the integral of $\cos(N\omega t_{\mathrm{cyc}})$ weighted with a smooth function of ω vanishes in the limit $N\to\infty$. This shows that, to leading order in the noise intensity, $R(m)\approx R_0(m)$, where

$$\begin{aligned} R_0(m) &= \frac{1}{2}(2r_1-1)^2t_{\mathrm{cyc}}^{-1}\tan^2\phi_R\sum_\ell S_q[\omega_\ell(m)] \\ &\quad\times\frac{1-\cos\omega_\ell(m)t_R}{\omega_\ell(m)^2} + R_C, \\ \omega_\ell(m) &= \frac{2\pi(m+\ell N)}{Nt_{\mathrm{cyc}}}, \end{aligned} \tag{54}$$

with

$$\begin{aligned} R_C &= 2r_1(1-r_1) - \frac{1}{4\pi}(2r_1-1)^2\tan^2\phi_R\int d\omega S_q(\omega) \\ &\quad\times\frac{1-\cos\omega t_R}{\omega^2}. \end{aligned} \tag{55}$$

In Eq. (54), the sum runs over positive and negative integer ℓ.

Equations (52) and (54) show an important advantageous feature of periodically repeated Ramsey measurements: the discrete Fourier transform of the measurement outcomes $\mathbb{E}[|X(m)|^2]$ provides an insight into the power spectrum of qubit frequency noise $S_q(\omega)$. One of the conditions to be met is that the noise should be weak, which can be inferred from the value of r_1.

If $S_q(\omega)$ increases with decreasing ω, as in the case of $1/f$ noise for example, for small m/N, a major contribution to $R_0(m)$ comes from the term with $\ell = 0$ in Eq. (54). In this case one can directly read off the frequency noise spectrum from $R_0(m)$ and thus ultimately from $\mathbb{E}[|X(m)|^2]$. However, generally, the situation is more complicated; disregarding the terms with $|\ell| > 0$ has to be taken with care.

VI. COMPARISON OF THE THEORY AND SIMULATIONS

In this section we present the results of simulations of periodically repeated Ramsey measurements and compare them with the theoretical predictions. The results are aimed at illustrating major qualitative aspects of the effect of low-frequency fluctuations of the qubit frequency on the measurements. We chose the ratio of the repetition period t_{cyc} to the accumulation time of the measurement t_R (see

Fig. 1) to be equal to $t_{\rm cyc}/t_R = 3$. Most of the results refer to $\phi_R = \pi/4$, where all centered correlators are "visible." For $\phi_R = 0$, we have $\tilde{r}_2 = 0$ in the case of weak noise, as seen from Eqs. (38) and (39). On the other hand, $\tilde{r}_3 = 0$ for $\phi_R = \pi/2$ in the case of Gaussian noise. We use $\phi_R = \pi/2$ for the noise from asymmetric TLSs to reveal the distinction from Gaussian noise. Also, we assume that t_R is much smaller than T_2 and disregard corrections $\propto t_R/T_2$.

We describe the centered correlators $\tilde{r}_2(k)$ and $\tilde{r}_3(k,\ell)$ found in long simulations, with the duration $Nt_{\rm cyc}$ much longer than the noise correlation time (the ergodic limit). Therefore, in terms of the results for TLSs, the initial distribution of TLSs has no effect: TLSs switch multiple times during the simulations. We use $N = 10^5$ and repeat the simulations 300 times to obtain good statistics.

In the subsections of this section we analyze the results for different types of TLSs and for Gaussian noise with different spectra. The simulation algorithms are outlined in Appendix B.

A. Effect of the coupling to symmetric TLSs

We present results of the simulations in which the coupling parameters are the same for all TLSs, $V^{(n)} = V$. We also assume that the switching rates $W_{ij}^{(n)}$ depend on n exponentially. For symmetric TLSs, where $W_{01}^{(n)} = W_{10}^{(n)} = W^{(n)}/2$, we choose

$$V^{(n)} = V, \qquad W^{(n)}t_R = \exp[-\alpha(n+n_0)].$$

This leads to spectrum $S_q(\omega)$ being of the $1/f$ form in a broad frequency range already for a comparatively small number of TLSs. This range depends on the values of n_0 and α; it also depends on the number of TLSs; see Appendix B. We study the parameter domain in which, for all TLSs, the condition $Nt_{\rm cyc} \gg W^{(n)}t_R$ for all n holds.

The goal of the simulations described in this section, besides testing the theory, is to explore how (i) the number of TLSs and (ii) the strength of the coupling of TLSs to the qubit affect correlators $\tilde{r}_2$ and $\tilde{r}_3$. Of special interest is also to find where the effects of the coupling to TLSs are mimicked by a Gaussian noise depending on the TLS parameters. Formally, the noise from a few TLSs is non-Gaussian. It becomes Gaussian in the limit where the number of TLSs is $N_{\rm TLS} \gg 1$, whereas the qubit coupling to an individual TLS is small, $V^{(n)} \propto N_{\rm TLS}^{-1/2}$. However, as we find, the actual conditions may be much less restrictive.

In Fig. 2 we show results for a qubit dispersively coupled to a set of ten symmetric TLSs. The left panel shows the evolution of $\tilde{r}_2(k)$ with the varying coupling strength V. The data and the theory are in excellent agreement. The simulated and calculated values of r_1 are also in excellent agreement, with the relative error $\lesssim 10^{-4}$. The results show that the decay of $\tilde{r}_2(k)$ with increasing k is (i) nonexponential and that (ii) it nonmonotonically depends on V. This is a consequence of two factors. First, while the contribution of an individual TLS to $\tilde{r}_2(k)$ decays with k exponentially, as seen from Eq. (19), $\tilde{r}_2(k)$ is determined by combinations of contributions from different TLSs, so that the overall decay becomes nonexponential. Second, for $V^{(n)} \gg W^{(n)}$, functions $\xi_k^{(n)}$ and $\Xi^{(n)}$ that determine $\tilde{r}_2(k)$ are combinations of $\sin V^{(n)}t_R$ and $\cos V^{(n)}t_R$. Therefore, they oscillate with the varying coupling strength. The inset demonstrates the oscillatory dependence of $\tilde{r}_2(k)$ on $V^{(n)} = V$ for $k = 1$.

The central panel in Fig. 2 presents a comparison of the fast Fourier transform (FFT) of the outcomes of the Ramsey measurements $\overline{|X(m)|^2}$ with the discrete Fourier transform $R(m)$ of $\tilde{r}_2(k)$ calculated from Eq. (19). Here $\overline{|X(m)|^2}$ is the value of $|X(m)|^2$ averaged over 300

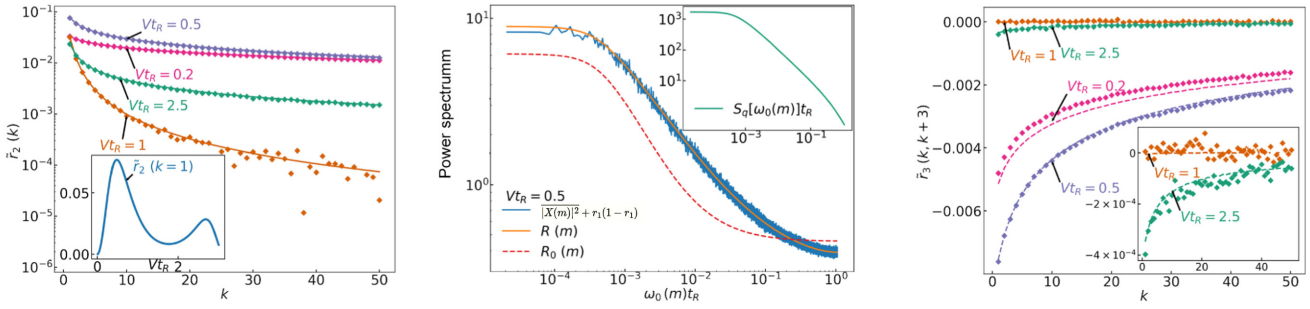

FIG. 2. Centered correlators of the measurement outcomes and the power spectrum for a qubit dispersively coupled to ten symmetric TLSs, $W_{01}^{(n)} = W_{10}^{(n)}$. The coupling is the same for all TLSs, $V^{(n)} = V$. The switching rates of the TLSs are $W^{(n)}t_R = \exp(-3n/4)$, $n = 1,\ldots,10$, and $\phi_R = \pi/4$. Diamonds show the results of simulations. Left panel: $\tilde{r}_2(k)$ for different coupling strength. Solid lines show the theory, Eq. (19). The inset shows $\tilde{r}_2(k)$ for $k = 1$ as a function of the coupling strengths. Central panel: power spectrum for coupling $Vt_R = 0.5$. The solid line shows the calculated discrete Fourier transform $R(m)$ of correlator $\tilde{r}_2$, Eq. (50), as a function of $\omega_0(m) = 2\pi m/Nt_{\rm cyc}$ for $N = 10^5$. The jagged line shows the averaged fast Fourier transform $|X(m)|^2$ [with added $r_1(1-r_1)$; cf. Eq. (52)] obtained from simulations. The dashed line shows the weak-noise limit of $R(m)$, Eq. (54). The inset shows the calculated power spectrum of the TLSs $S_q[\omega_0(m)]$. Right panel: comparison of the centered correlator $\tilde{r}_3(k,k+3)$ obtained from the simulated data with the results obtained assuming that the noise has Gaussian statistics.

simulations. The FFT and the theory are in excellent agreement. They both display a characteristic shape, which is reminiscent of the shape of the power spectrum of the TLS-induced noise $S_q(\omega)$ shown in the inset. At the same time, there are significant differences between the shape of the FFT and $S_q(\omega)$. The dashed line shows that the weak-noise approximation $R_0(m)$ is also noticeably different from $R(m)$ for the chosen coupling $Vt_R = 0.5$.

The data in the right panel of Fig. 2 are fairly unexpected. The plot for ten TLSs compares the directly simulated third correlator $\tilde{r}_3(k,l)$ with the results for $\tilde{r}_3(k,l)$ "constructed" from the data on r_1 and $\tilde{r}_2(k)$ by assuming that the noise from the TLSs is Gaussian. The construction goes as follows: if the noise is Gaussian, from the data on r_1 and $\tilde{r}_2(k)$ one can unambiguously determine the Gaussian noise correlators f_k, Eq. (36). They fully determine all properties of the Gaussian noise and, in particular, give $\tilde{r}_3(k,l)$; cf. Eq. (39). This is the case for an arbitrary coupling. We call $\tilde{r}_3$ found this way the *"constructed Gaussian."* When applied to the noise from ten TLSs, the constructed $\tilde{r}_3(k,l)$ is in good agreement with the direct simulations. This is an indication that, already for ten TLSs, the TLS-induced fluctuations mimic fluctuations induced by Gaussian noise in a broad range of the coupling strength.

A strong extra argument in favor of the Gaussianity is provided by the data for $\phi_R = \pi/2$. In the Gaussian approximation one expects that $\tilde{r}_3 = 0$ for $\phi_R = \pi/2$. Our simulations of this case for the set of ten TLSs with the same parameters as above show that $\tilde{r}_3$ is indeed exceedingly small, $|\tilde{r}_3(k,k+3)| < 10^{-4}$, whereas r_1 and $\tilde{r}_2(k)$ are in excellent agreement with the theory; see Appendix D.

Figure 3 presents the results of the analysis similar to that in Fig. 2, but for one TLS. The results of the simulations are again in excellent agreement with the theory. The left panel shows that, for one TLS, the decay of simulated $\tilde{r}_2(k)$ with the increasing k is perfectly exponential, as expected from Eq. (19). For the chosen parameters, the ratio V/W is ≥ 50 for all values of Vt_R in the main plot, so that the results are in good agreement with the strong-coupling expression (34). The sinusoidal dependence $\tilde{r}_2(k) \propto \sin^2(Vt_R)$ as given by this expression is in good agreement with the full expression (19) plotted in the inset.

The central panel shows that, for one TLS and for the considered coupling $Vt_R = 0.5$, the simulated FFT not only agrees with the calculated discrete Fourier transform $R(m)$, but is fairly close to the result of the weak-coupling limit $R_0(m)$, even though Vt_R is not that small. This is significantly different from the case of ten TLSs shown in Fig. 2. For a larger number of TLSs, the overall coupling to the qubit is stronger than for one TLS even where the coupling of each TLS to the qubit is the same.

The right panel shows that $\tilde{r}_3(k,k+3)$ is very small for one symmetric TLS. It is essentially within simulation noise, $|\tilde{r}_3| \lesssim 10^{-4}$. Most importantly, if the TLS-induced noise is assumed Gaussian and $\tilde{r}_3$ is constructed based on the values of r_1 and $\tilde{r}_2(k)$, the result for $\tilde{r}_3(k,l)$ is strongly different from the simulations. Moreover, it is impossible to perform such a construction for $Vt_R = 2.5$, since in this case $r_1 < 0.5$, which is incompatible with the assumption that the noise is Gaussian; cf. Eq. (38). Therefore, for one TLS, correlator $\tilde{r}_3$ unambiguously shows that the TLS-induced noise is non-Gaussian.

B. Asymmetric TLSs

The effect of asymmetry of TLSs on the qubit frequency noise has not been carefully explored, to the best of our knowledge. Meanwhile, if the energy difference between states $|0\rangle$ and $|1\rangle$ of a TLS is comparable or exceeds k_BT, rates W_{01} and W_{10} are significantly different, thus making a TLS asymmetric. Therefore, it is important to understand the role of the asymmetry.

One of the central questions is whether the asymmetry makes the noise more "non-Gaussian" even where the number of TLSs is not small. One may expect this to be the case based on the result of the perturbation theory in Sec. III E. For weak zero-mean Gaussian noise, $\tilde{r}_3(k,l)$ is of second order in the noise intensity [see Eq. (40)], i.e.,

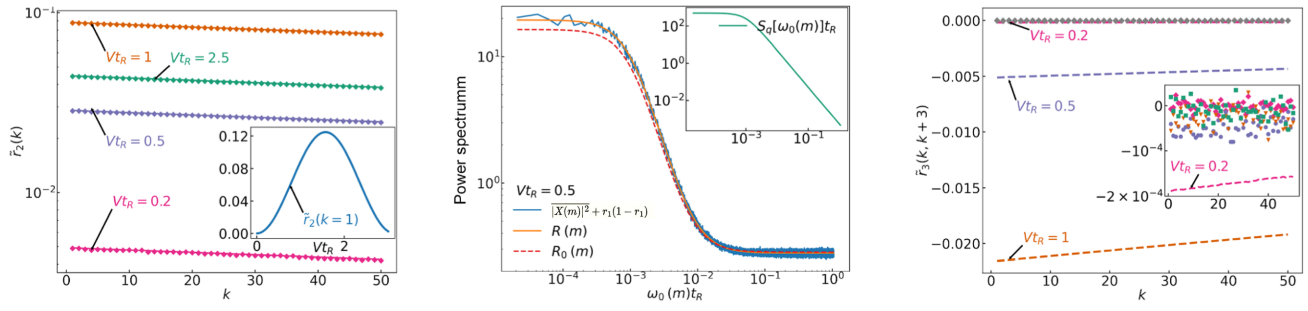

FIG. 3. The same as in Fig. 2 but for the coupling to one symmetric TLS, $Wt_R = 0.001$. The inset in the right panel shows the simulated values of $\tilde{r}_3(k,k+3)$ for $Vt_R = 0.2, 0.5, 1$, and 2.5 (diamonds, circles, triangles, and squares, respectively). The data are noisy at the level of 10^{-4}.

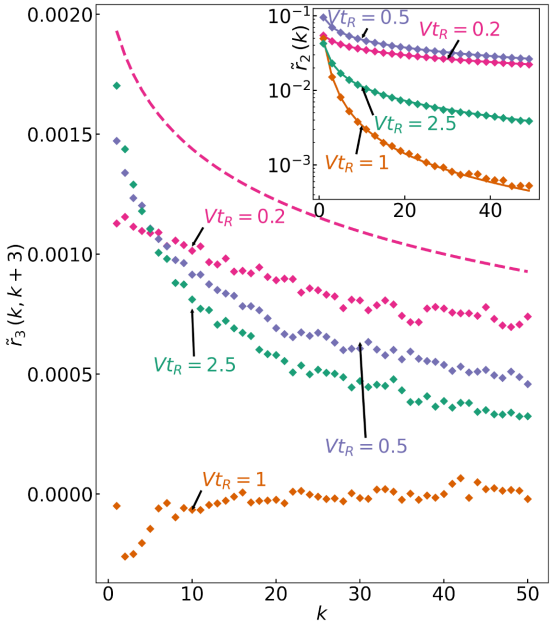

FIG. 4. Centered correlator $\tilde{r}_3(k, k+3)$ for ten asymmetric TLSs with $W_{01}^{(n)} t_R = \exp[-3(n+1)/4]/2$ and $W_{10}^{(n)} t_R = \exp(-3n/4)/2$, $n = 1, \ldots, 10$. The coupling is assumed to be the same for all TLSs, $V^{(n)} = V$, and $\phi_R = \pi/2$. For the weak coupling, $Vt_R = 0.2$, we also show with the dashed line the weak coupling approximation, Eq. (31). The inset presents the results of simulations (diamonds) and the theory (solid lines) for the centered correlator $\tilde{r}_2(k)$.

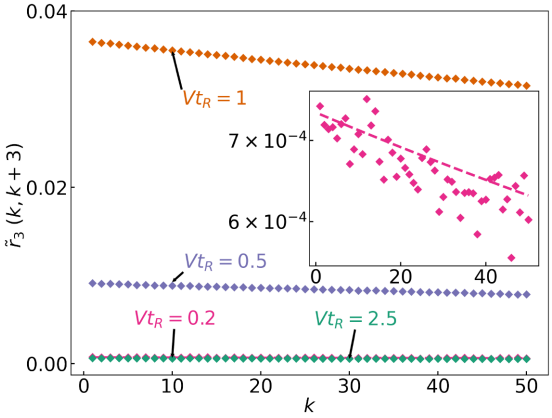

FIG. 5. Centered correlator $\tilde{r}_3(k, k+3)$ for one asymmetric TLS with $W_{10} t_R = 0.00075$ and $W_{01} t_R = 0.00025$ for $\phi_R = \pi/2$. The data for $Vt_R = 0.2$ and $Vt_R = 2.5$ are overlapping on the chosen scale. Inset: enlarged view of the weak coupling limit, where the comparison with Eq. (31) is represented by the dashed line.

of fourth order in the coupling, whereas for asymmetric TLSs, it becomes nonzero already at third order in the coupling.

A direct way to reveal non-Gaussianity, as mentioned earlier, is to study $\tilde{r}_3(k, l)$ for $\phi_R = \pi/2$, as $\tilde{r}_3(k, l) = 0$ for Gaussian noise. In this subsection we present the results of simulations of the effect of asymmetric TLSs for $\phi_R = \pi/2$.

In Fig. 4 we show the results for ten TLSs. It is seen that, in contrast to the case of symmetric TLSs presented in Appendix D, $\tilde{r}_3$ is nonzero. It is a nonmonotonic function of the coupling strength and even changes sign with varying Vt_R. The decay of $\tilde{r}_3(k, k+3)$ is nonexponential, and the decay rate strongly depends on the coupling strength as well. Even for $Vt_R = 0.2$, there is a significant difference between the data and expression (31) for $\tilde{r}_3$ in the weak-coupling limit, which is shown by the dashed line. This is because weak coupling of individual TLSs does not translate into weak coupling of a few TLSs taken together. The inset demonstrates excellent agreement between the simulation results and the full theory for $\tilde{r}_2(k)$.

Figure 5 presents the data on the coupling to a single asymmetric TLS. Such coupling also leads to a nonzero $\tilde{r}_3$ for $\phi_R = \pi/2$, as in the case of many TLSs. Interestingly, $\tilde{r}_3(k, k+3)$ decays with increasing k slowly, generally slower than in the case of ten TLSs. As seen from the inset, for one TLS, the asymptotic expression (31) well describes $\tilde{r}_3$ for the comparatively weak coupling $Vt_R = 0.2$.

The results of this subsection demonstrate a significant difference between the effects of the coupling to symmetric and asymmetric TLSs. Studying the three-time correlator $\tilde{r}_3$ is a sensitive tool for revealing the asymmetry, in combination with the studies of the lower-order correlators and their decay.

C. Effect of Gaussian noise

For Gaussian noise, the values of the correlators of the measurement outcomes $r_2(k)$ and $r_3(k, \ell)$, as well as the higher-order correlators are determined by the single set of parameters f_k, which are simply expressed in terms of the noise power spectrum; see Eqs. (26) and (36). The theory is presented in Sec. IV. Here we present the results of the simulations for exponentially correlated noise and for noise with the $1/f$ -type power spectrum given by Eq. (46). The exponentially correlated noise is characterized by the correlation time $\tau_{\rm corr}$, whereas the $1/f$ noise we study is characterized by a soft-cutoff minimal frequency $\omega_{\rm min}$. For both types of noise, the simulated values of the probability r_1 to have "1" as an outcome of the measurements coincided with the theoretical values to an accuracy $\lesssim 10^{-4}$.

In Fig. 6 we show the results for the centered correlators $\tilde{r}_2(k)$ and $\tilde{r}_3(k, k+3)$ for the exponentially correlated noise; its power spectrum is $S_q(\omega) = D_{\rm corr}/(1 + \omega^2 \tau_{\rm corr}^2)$; cf. Eq. (42). The plots refer to a comparatively weak coupling. For such coupling, as expected from the theoretical arguments, $\tilde{r}_2(k)$ falls off exponentially with k, i.e., the two-time correlator decays exponentially with time $kt_{\rm cyc}$.

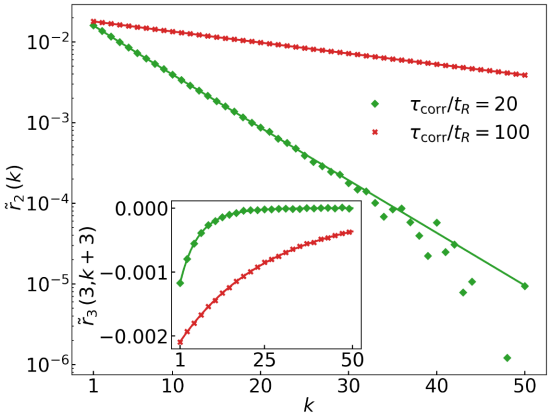

FIG. 6. Two- and three-time centered correlators $\tilde{r}_2(k)$ (main plot) and $\tilde{r}_3(k, k+3)$ (inset) for exponentially correlated noise. The solid lines show the theory, Eqs. (38), (39), and (43). The crosses (red) and diamonds (green) show the simulations. The noise intensity and the correlation time for the green and red data are $D_{corr} = 6.51$, $\tau_{corr}/t_R = 20$ and $D_{corr} = 32.11$, $\tau_{corr}/t_R = 100$, respectively. They are adjusted to give the same value of parameter f_0, which characterizes the coupling strength and determines probability r_1, Eq. (38), $f_0 = 0.16$.

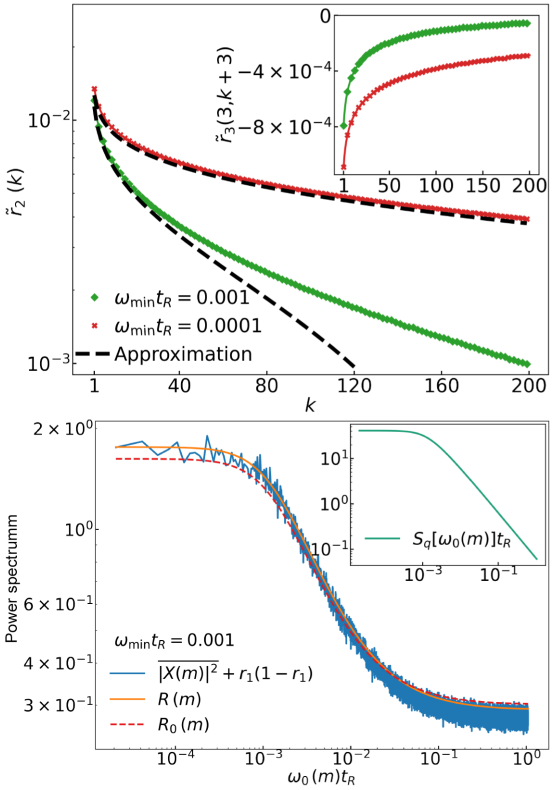

FIG. 7. Top panel: centered correlators $\tilde{r}_2(k)$ (main plot) and $\tilde{r}_3(k, k+3)$ (inset) for $1/f$ -type noise with spectrum (46); ω_{min} is the smooth low-frequency cutoff. The solid lines show the theory and the crosses and diamonds show the simulations. The dashed lines show the intermediate-time approximation (49). The noise intensities for the green (diamonds) and red (crosses) data are $D_{fl} = 0.0642$ and 0.03158, respectively. They are adjusted so that parameter f_0, which characterizes the coupling strength, is the same, $f_0 = 0.16$. Bottom panel: power spectrum for $\omega_{min}t_R = 0.001$ obtained as the FFT of the data (jagged line) averaged over 300 realizations of 10^5 measurements. The solid line shows the discrete Fourier transform $R(m)$ of the analytical expression (38) for $\tilde{r}_2(k)$, whereas $R_0(m)$ shows the weak coupling limit of $R(m)$, Eq. (54). The inset shows the power spectrum $S_q(\omega)$ of the studied Gaussian noise.

The decay rate is determined by the decay rate of noise correlations τ_{corr}^{-1}. However, the three-time correlator decays nonexponentially. This feature demonstrates the importance of studying a three-time correlator in order to identify and characterize noise.

In Fig. 7 we show the centered correlators for model (46) of $1/f$ noise. In contrast to the results for the exponentially correlated noise in Fig. 6, $\tilde{r}_2(k)$ does not fall off exponentially with increasing k for comparatively small k even for weak noise. However, it approaches exponential decay for large k, where $k\omega_{min}t_{cyc} \gg 1$, with the exponent determined by the low-frequency cutoff ω_{min}. For small $\omega_{min}t_{cyc}$, this range is practically inaccessible, as $\tilde{r}_2(k)$ becomes extremely small. The dependence of $\tilde{r}_2(k)$ on k is close to logarithmic for $t_R \ll kt_{cyc} \ll 1/\omega_{min}$. The corresponding expression (49) is shown by the dashed lines. As seen from the figure, approximation (49) actually requires a more stringent condition, $\omega_{min}kt_{cyc} \lesssim 0.1$.

The centered three-time correlator $\tilde{r}_3(k, \ell)$ displays a characteristic dependence on k and ℓ for $1/f$ noise, which can be inferred from the general expressions (39) and (47). As seen from the comparison of Figs. 6 and 7, this dependence is very different for Gaussian exponentially correlated noise and $1/f$ noise.

The bottom panel of Fig. 7 shows the power spectrum of the outcomes of the repeated Ramsey measurements for $1/f$ -type noise. The data are in excellent agreement with the theoretical discrete Fourier transform $R(m)$ of $\tilde{r}_2(k)$ and, for the studied noise intensity, are in reasonable agreement with the weak-noise approximation $R_0(m)$. The data also show that, even for the studied weak noise, the spectrum $\overline{|X(m)|^2}$ is noticeably different from the noise spectrum except for a relatively narrow range, where both fall off as $1/f$. This is an important feature, in terms of noise characterization. It comes about because the contribution of the terms with $|\ell| > 0$ in Eq. (54) increases with increasing frequency $\omega_0(m)$.

VII. THE MASTER EQUATION

We now proceed with describing the method used to derive the results for the correlators of the periodically repeated Ramsey measurements presented in Secs. III and IV.

A. The Hamiltonian

We consider a qubit, which is coupled to TLSs, has a fluctuating frequency, and is subjected to the control pulses as shown in Fig. 1. The qubit Hamiltonian is $H = H_q + H_{q-\mathrm{TLS}}$. Here $H_{q-\mathrm{TLS}}$ is given by Eq. (9) and describes the dispersive coupling to TLSs, whereas H_q has the form

$$H_q = -\frac{1}{2}\delta\omega_q(t)\sigma_z + \frac{\pi}{4}\sigma_y \sum_k [\delta(t - kt_{\mathrm{cyc}}) + \delta(t - kt_{\mathrm{cyc}} - t_R)]. \quad (56)$$

The term $\propto \sigma_y$ in Eq. (56) describes the periodically repeated pairs of Ramsey pulses for rotation about the y axis, whereas $\delta\omega_q(t)$ describes the qubit frequency fluctuations due to external classical noise. Here we somewhat conditionally distinguish such classical noise from noise stemming from the coupling to TLSs; see however Appendix A where the effect of TLSs is described by modeling $\delta\omega_q(t)$ by a telegraph noise

As indicated before, we assume that $\langle\delta\omega_q(t)\rangle = 0$. If $\langle\delta\omega_q(t)\rangle$ were nonzero, it would be incorporated into the mean qubit frequency ω_q measured in the experiment. The detuning of $\delta\omega_q$ from frequency ω_{ref} of the reference signal used in the Ramsey measurements leads to a phase accumulation ϕ_R during a measurement, as described by Eq. (8). Phase ϕ_R can be controlled in the experiment by varying ω_{ref} or, alternatively, can be implemented by incorporating into H_q the term

$$H_R = -\frac{1}{2}\phi_R\sigma_z \sum_{k\geq 0} \delta(t - kt_{\mathrm{cyc}} - t_R^-). \quad (57)$$

Here and below the superscript "+" or "−" after the time argument has the following meaning:

$$t^{\pm} \equiv t \pm \epsilon, \qquad \epsilon \to +0.$$

Hamiltonian H_R describes rotations of the qubit around the z axis prior to the second Ramsey pulse within a cycle, i.e., the pulse applied at time $kt_{\mathrm{cyc}} + t_R$; see Eq. (56) and also Fig. 1.

The operator of the qubit frequency shift due to the coupling to TLSs $\sum_n V^{(n)}\hat{\tau}_z^{(n)}$ has a nonzero expectation value. Therefore we define the frequency noise operator $\delta\hat{\omega}_q$ by Eq. (10) so that $\langle\delta\hat{\omega}_q\rangle = 0$. Equivalently, one could consider the qubit-TLS coupling of the form

$$H'_{q-\mathrm{TLS}} = -\frac{1}{2}\sigma_z \sum_n V^{(n)}(\hat{\tau}_z^{(n)} - \langle\hat{\tau}_z^{(n)}\rangle), \quad (58)$$

which does not lead to a renormalization of the mean qubit frequency. In this sense it is more relevant from the viewpoint of the experiment. If the coupling Hamiltonian is of form (58), in Eq. (57) one should use ϕ_R rather than the phase $\tilde{\phi}_R$ defined by Eq. (17). However, in the calculations we use the more conventional form of the coupling, which is given by Eq. (9).

To analyze the dephasing due to the dispersive coupling to TLSs, Eq. (9), we write the states of an nth TLS as

$$|0\rangle^{(n)} \equiv \begin{pmatrix}1\\0\end{pmatrix}^{(n)}, \qquad |1\rangle^{(n)} \equiv \begin{pmatrix}0\\1\end{pmatrix}^{(n)},$$

and we use the Pauli operators $\hat{\tau}_{\varkappa}^{(n)}$ to describe the TLS dynamics. Here $\varkappa = 0, x, y, z$, with $\hat{\tau}_0^{(n)} \equiv \hat{I}_{\tau}^{(n)}$ being the identity operator.

B. Dynamics during a Ramsey measurement

We first consider the qubit dynamics during a Ramsey measurement, i.e., in the time interval $kt_{\mathrm{cyc}} < t < kt_{\mathrm{cyc}} + t_R$; cf. Fig. 1. We assume that, in slow time compared to $1/\omega_{\mathrm{ref}}$, relaxation of the qubit and TLSs is Markovian. The kinetic equation for the density matrix then has the standard form

$$\partial_t\rho = i[\rho, H_q + H_{q-\mathrm{TLS}}] + 2\Gamma\mathcal{D}[\sigma_+]\rho + \frac{1}{2}\Gamma_\phi\mathcal{D}[\sigma_z]\rho + \sum_n \mathcal{L}_{\mathrm{TLS}}^{(n)}\rho, \quad (59)$$

where the last term describes the relaxation of TLSs,

$$\mathcal{L}_{\mathrm{TLS}}^{(n)}\rho = W_{10}^{(n)}\mathcal{D}[\hat{\tau}_+^{(n)}]\rho + W_{01}^{(n)}\mathcal{D}[\hat{\tau}_-^{(n)}]\rho + \tfrac{1}{2}\Gamma_{\phi\mathrm{TLS}}^{(n)}\mathcal{D}[\hat{\tau}_z^{(n)}]\rho. \quad (60)$$

We use the conventional notation $\mathcal{D}[F]\rho = F\rho F^\dagger - (F^\dagger F\rho + \rho F^\dagger F)/2$ for the relaxation operator; $\sigma_\pm = (\sigma_x \pm i\sigma_y)/2$, $\hat{\tau}_\pm^{(n)} = (\hat{\tau}_x^{(n)} \pm i\hat{\tau}_y^{(n)})/2$.

Parameters Γ and Γ_ϕ describe the qubit decay rate and the rate of qubit dephasing due to fast dephasing processes. They give the familiar parameters of the Bloch equation for the qubit,

$$T_1 = 1/2\Gamma, \qquad T_2 = 1/(\Gamma + \Gamma_\phi).$$

Parameters $W_{ij}^{(n)}$ describe the rates of transitions $|i\rangle^{(n)} \to |j\rangle^{(n)}$ between the states of an nth TLS (i,j take on values $0, 1$), whereas $\Gamma_{\phi\mathrm{TLS}}^{(n)}$ is the TLS dephasing rate. To make the TLSs fully incoherent, this rate has to be much larger than the switching rates. In this case the off-diagonal matrix elements of ρ with respect to the TLS states, ${}^{(n)}\langle i|\,\rho\,|j\rangle^{(n)}$ with $i \neq j$, will decay fast and can be disregarded. As seen from the analysis below, for the considered dispersive qubit-to-TLS coupling, these matrix elements do not affect the outcomes of qubit measurements. Therefore, they will not be discussed, i.e., we consider only the matrix elements ${}^{(n)}\langle i|\,\rho\,|j\rangle^{(n)}$ with $i = j$.

It is assumed in Eq. (60) that each TLS is coupled to its individual thermal reservoir, that is, not only is there no direct interaction between TLSs, but there is also no interaction mediated by a common thermal reservoir. In the case of phononic thermal reservoirs, this model goes back to the original papers [49,50].

Another important assumption implicit in the model is that the switching rates $W_{ij}^{(n)}$ are independent of the qubit state. This is somewhat similar to the neglect of the effect of the TLS-to-TLS coupling in Refs. [49,50]. Generally, the dispersive coupling to a qubit shifts the TLS energy levels, which may invalidate the approximation. However, the effect of this shift on the switching rates is small in many cases of interest. Familiar examples are the case where the TLS dephasing rates exceed the shifts or the case where the switching of TLSs is thermally activated and the qubit-state-dependent shift is smaller than k_BT. Disregarding the qubit-induced change of the switching rates is essentially equivalent to disregarding the backaction from the coupling to a qubit.

1. Solution of the master equation

We assume that at $t = 0^-$, i.e., just before the first $\pi/2$ rotation about the y axis, the qubit is in the ground state $|0\rangle$ and the TLSs are in their stationary states. From Eq. (60), the stationary density matrix of an nth TLS is

$$\rho_{\rm st}^{(n)} = \frac{1}{2}\left[\hat{I}^{(n)} + \frac{\Delta W^{(n)}}{W^{(n)}}\hat{\tau}_z^{(n)}\right],$$
$$W^{(n)} = W_{01}^{(n)} + W_{10}^{(n)}, \qquad \Delta W^{(n)} = W_{10}^{(n)} - W_{01}^{(n)}. \quad (61)$$

The density matrix of the whole system, the qubit, and TLSs, before the first rotation around the y axis is

$$\rho(t = 0^-) = \frac{1}{2}(\hat{I}_q + \sigma_z)\prod_n \rho_{\rm st}^{(n)}.$$

The rotation of the qubit at $t = 0$ is described by the term $\propto \sigma_y$ with $k = 0$ in Hamiltonian (56). TLSs are not affected by unitary transformations on the qubit. The density matrix after the transformation becomes

$$\rho(t = 0^+) = \frac{1}{2}(\hat{I}_q + \sigma_x)\prod_n \rho_{\rm st}^{(n)}. \quad (62)$$

This equation provides the initial condition for the evolution of the density matrix during the first Ramsey measurement, i.e., in the time interval $0 < t < t_R$. The solution of Eq. (59) in this time interval can be sought in the form

$$\rho(t) = \frac{1}{2}(\hat{I}_q + \sigma_z)\rho_I + \frac{1}{2}e^{-t/T_1}\sigma_z\rho_z + \frac{1}{2}e^{-t/T_2}\sum_{\alpha=\pm}\exp\left[i\alpha\int_0^t dt'\delta\omega_q(t')\right]\sigma_\alpha\rho_\alpha \quad (63)$$

with operators ρ_λ defined as

$$\rho_\lambda = \prod_n \sum_{\varkappa=0,z} C_{\lambda\varkappa}^{(n)}\hat{\tau}_\varkappa^{(n)}. \quad (64)$$

Here $\lambda = I, z, \pm$ enumerates the components of the qubit-dependent part of the density matrix, whereas $\varkappa = 0, z$ enumerates the TLS operators $\hat{\tau}_0^{(n)} \equiv \hat{I}^{(n)}$ and $\hat{\tau}_z^{(n)}$. Operators ρ_λ depend only on the TLS variables. Coefficients $C_{\lambda\varkappa}^{(n)} \equiv C_{\lambda\varkappa}^{(n)}(t)$ describe the evolution of the density matrix in time.

The components of the density matrix ρ that contain $\hat{\tau}_\pm^{(n)}$ are uncoupled from other components of ρ. They do not get coupled by the coupling to the qubit and by the gate operations on the qubit. They decay with rates $W^{(n)} + \Gamma_{\phi{\rm TLS}}^{(n)}$ and, as indicated earlier, will not be discussed. This explains why $\varkappa$ in Eq. (64) runs through 0 and z only.

The equations for $C_{\lambda\varkappa}^{(n)}$ are obtained by substituting Eq. (63) into the full master equation (59), multiplying the left- and right-hand sides in turn by $\hat{I}_q, \hat{I}_q - \sigma_z, \sigma_\pm$, and taking a trace over the qubit states. Because the TLSs' decays are independent of each other, the resulting equations for ρ_λ separate into equations for individual TLSs (see Appendix E). Equations (60) and (63) then reduce to the equation

$$\sum_\varkappa \dot{C}_{\lambda\varkappa}^{(n)}\hat{\tau}_\varkappa^{(n)} = \mathcal{L}_{\rm TLS}^{(n)}\sum_\varkappa C_{\lambda\varkappa}^{(n)}\hat{\tau}_\varkappa^{(n)} + i\sum_{\alpha=\pm}\delta_{\lambda\alpha}\alpha V^{(n)}(C_{\alpha 0}^{(n)}\hat{\tau}_z^{(n)} + C_{\alpha z}^{(n)}\hat{\tau}_0^{(n)}) \quad (65)$$

with $\varkappa = 0, z$. Multiplying this equation in turn by the TLS operators $\hat{I}^{(n)}$ and $\hat{\tau}_z^{(n)}$ and taking a trace over the TLS states, we obtain equations for each of the coefficients $C_{\lambda\varkappa}^{(n)}$.

The last term in Eq. (65) describes the effect of the coupling to the qubit on the TLS dynamics. This term comes from the components of the density matrix ρ, which are proportional to $\sigma_\pm$. It determines the accumulation of the phase of the qubit between the Ramsey pulses at $t = 0$ and $t = t_R$.

The initial conditions for $C_{\lambda\varkappa}^{(n)}$ follow from Eq. (62) and are given by Eq. (E7) in Appendix E. Coefficients $C_{\lambda\varkappa}^{(n)}(t)$ in terms of $C_{\lambda\varkappa}^{(n)}(0)$ are given by Eqs. (E4) and (E5). Using the expressions for $C_{\lambda\varkappa}^{(n)}(t)$, we find that, by the end of the interval between the Ramsey pulses, i.e., for $t \to t_R^-$, we have

$$C_{I0}^{(n)}(t_R) = \tfrac{1}{2}, \qquad C_{+0}^{(n)}(t_R) = \tfrac{1}{2}\Xi^{(n)}(t_R), \quad (66)$$

where function $\Xi_n(t_R)$ is given in Eq. (16). This function describes the effect of the coupling to an nth TLS on the probability of the Ramsey measurement outcome. It depends on the interrelation between the strength of the

TLS-to-qubit coupling $V^{(n)}$ and the TLS relaxation rate $W^{(n)}$, that is, for a TLS to be effectively strongly coupled to the qubit, it is necessary to have $|V^{(n)}|$ large compared to the TLS relaxation rate $W^{(n)}$.

The explicit expressions for coefficients $C^{(n)}_{\lambda\varkappa}(t_R)$ determine operators $\rho_\lambda(t_R)$, as seen from Eq. (64). They thus describe the change of the density matrix $\rho(t)$ over the time after the qubit was prepared in state $(|0\rangle + |1\rangle)/\sqrt{2}$ and before it is going to be measured.

C. The outcome probability of the first Ramsey measurement

The above results allow us to find the probability r_1 of obtaining "1" as an outcome of the Ramsey measurement. In the Bloch sphere representation, the involved steps include the rotation of the density matrix $\rho(t_R)$ about the z axis by an angle $\tilde{\phi}_R$. The corresponding unitary transformation is determined by Eq. (57), in which we replace ϕ_R with $\tilde{\phi}_R$ to allow for the shift of the average qubit frequency due to the coupling to TLSs.

The rotation about the z axis is followed by the rotation about the y axis by $\pi/2$, as prescribed by the term $(\pi/4)\sigma_y\delta(t-t_R)$ in Eq. (56). Finally, the transformed density matrix right after this rotation $\rho(t_R^+)$ has to be multiplied by the operator $\hat{P} = (\hat{I}_q - \sigma_z)/2$ and the trace over the states of the qubit and the TLSs has to be taken along with the averaging over classical noise of the qubit frequency $\delta\omega_q$.

The aforementioned unitary transformations refer to the operators $\sigma_{x,y,z}$ in the density matrix $\rho(t)$ in Eq. (63). Operators $\rho_\lambda(t_R)$ are operators in the space of TLSs; they are not affected by the gate operations on the qubit at time t_R, i.e., $\rho_\lambda(t_R^-) = \rho_\lambda(t_R^+) = \rho_\lambda(t_R)$ (recall that λ takes on values $I, z, \pm$) . In terms of these operators

$$\hat{P}\rho(t_R^+) = \mathfrak{R}(t_R^+) + \hat{m},$$
$$\mathfrak{R}(t) = \frac{1}{4}(\hat{I}_q + \sigma_z)\left[\rho_I(t) + \frac{1}{2}e^{-t/T_2}\sum_\alpha e^{i\alpha(\theta+\tilde{\phi}_R)}\rho_\alpha(t)\right]. \tag{67}$$

Here, $\hat{m}$ is a sum of the terms proportional to σ_x, σ_y, and σ_z; therefore, $\mathrm{Tr}\,\hat{m} = 0$. The term $\theta = \int_0^{t_R}\delta\omega_q(t)dt$ is the phase accumulated because of slow classical qubit frequency noise. It *does not* include the contribution from TLSs.

From Eqs. (66) and (67) we find that the probability of obtaining "1" in a Ramsey measurement is given by Eq. (15). To allow for a classical qubit frequency noise, one has to replace the factor $\exp(i\tilde{\phi}_R)$ in Eq. (15),

$$\exp(i\tilde{\phi}_R) \to \exp(i\tilde{\phi}_R)\langle e^{i\theta}\rangle, \tag{68}$$

where $\langle\cdot\rangle$ implies averaging over the classical frequency noise. This noise does not affect the dynamics of TLSs and therefore its effect is just described by an extra factor.

VIII. THE PAIR CORRELATION FUNCTION FOR THE COUPLING TO TWO-LEVEL SYSTEMS

In this section we discuss the effect of TLSs on the pair correlation function of the qubit measurements $r_2(k)$. To simplify the notation, we disregard the classical noise, i.e., consider the qubit frequency modulation due to TLSs only. We start with the correlator for neighboring cycles, i.e., $r_2(1)$, and, as we move on, we extend the analysis to $r_2(k)$ for an arbitrary k.

It is clear from definition (3) that finding $r_2(1)$ involves the following steps. After we find $\hat{P}\rho(t_R^+)$, we have to find how the density matrix of the qubit + TLSs, which at time t_R^+ is given by $\hat{P}\rho(t_R^+)$, evolves in the time interval from t_R^+ to $t_{\rm cyc}$. In this time interval the qubit is reset to the ground state $|0\rangle$. At $t_{\rm cyc}$ the qubit is rotated to $(|0\rangle + |1\rangle)/\sqrt{2}$. We then have to consider the dynamics in the interval from $t_{\rm cyc}^+$ to $t_{\rm cyc}^+ + t_R$. At $t_{\rm cyc} + t_R$ the qubit is again rotated and the evolved operator $\rho(t_{\rm cyc} + t_R^+)$ is multiplied by $\hat{P}$. The value of $r_2(1)$ is given by the trace of the result. We discuss each of these steps separately.

A. Evolution during the reset, $t_R < t < t_{\rm cyc}$

The dynamics of the system during the reset of the qubit can be formally described by the master equation (59) with initial condition $\hat{P}\rho(t_R^+)$. In this equation one can assume that the qubit decay rate Γ is large in this time range, $\Gamma(t_{\rm cyc} - t_R) \gg 1$. In this limit the part of $\rho(t)$ that comes from operator $\hat{m}$ and is thus proportional to $\sigma_{x,y,z}$ will decay to zero. Therefore, only the evolution of operator $\mathfrak{R}(t)$ in Eq. (67) is of interest.

In operator $\mathfrak{R}(t)$ the qubit-dependent factor $\hat{I} + \sigma_z$ does not change. However, the TLSs are not in their stationary states at t_R, and they keep evolving for $t > t_R$, each with its own rate. To describe this evolution, it is convenient to first separate out the part $\mathfrak{R}_{\rm st}$ of $\mathfrak{R}(t)$ that would describe the system if the TLSs were in the stationary states, i.e., if they were described by the density matrices $\rho_{\rm st}^{(n)}$. Using the explicit expressions (66), (E8), and (E9) for operators $\rho_I, \rho_\pm$, we obtain

$$\mathfrak{R}(t) = r_1\mathfrak{R}_{\rm st}(t) + \mathfrak{R}_{\rm corr}(t), \qquad t_R^+ \le t < t_{\rm cyc},$$
$$\mathfrak{R}_{\rm st}(t_R) = \frac{1}{2}(\hat{I}_q + \sigma_z)\prod_n \rho_{\rm st}^{(n)}, \tag{69}$$

and

$$\mathfrak{R}_{\rm corr}(t_R) = \frac{1}{2}(\hat{I}_q + \sigma_z) \times \sum_{s\geq 1}^{N_{\rm TLS}} \sum_{\{m\}_s} \mathbb{K}_{\{m\}_s} \hat{\tau}_z^{(m_1)} \cdots \hat{\tau}_z^{(m_s)} \prod_{n\notin\{m\}_s} \rho_{\rm st}^{(n)}. \tag{70}$$

Here we have introduced sets of TLSs $\{m\}_s$. Their components $m_1, m_2, \ldots, m_s$ enumerate different TLSs. The values of m_i $(i = 1, \ldots, s)$ within each set run from 1 to $N_{\rm TLS}$. The sum $\sum_{\{m\}_s}$ is taken over all m_i; for example, one can think of it as

$$\sum_{\{m\}_s} \equiv \sum_{N_{\rm TLS}\geq m_1 > m_2 > \cdots > m_s \geq 1}.$$

The parameters $\mathbb{K}_{m_s}$ are given in Appendix F.

The form of $\mathfrak{R}_{\rm corr}$ can be understood by noting that, to describe the evolution of $\mathfrak{R}(t)$, we have to take into account the decay of all possible combinations of TLSs. The parameter s in Eq. (70) gives the number of TLSs included in a combination, $1 \leq s \leq N_{\rm TLS}$. Note that, by construction, the trace over the TLS states of any term in the sum over s is equal to zero. Operator $\mathfrak{R}_{\rm st}(t)$ describes the qubit in its ground state and the TLSs in their stationary states. It is not changed during reset, i.e.,

$$\mathfrak{R}_{\rm st}(t_{\rm cyc}^-) = \mathfrak{R}_{\rm st}(t_R^+).$$

In contrast, the TLS operators $\hat{\tau}_z^{(m_i)}$ in $\mathfrak{R}_{\rm corr}$ exponentially decay with rates $W^{(m_i)}$ because of the transitions between the states of the TLSs, as seen from Eq. (60). Since the TLSs are independent, over the duration of the reset $t_{\rm cyc} - t_R$ each $\hat{\tau}_z^{(m_i)}$ in Eq. (70) acquires a factor $\exp[-W^{(m_i)}(t_{\rm cyc} - t_R)]$, so that at the end of the reset period, i.e., at the end of the cycle, the expression for $\mathfrak{R}_{\rm corr}(t_{\rm cyc}^-)$ is given by Eq. (70), in which one replaces

$$\hat{\tau}_z^{(m_i)} \to \hat{\tau}_z^{(m_i)} \exp[-W^{(m_i)}(t_{\rm cyc} - t_R)] \tag{71}$$

for all $m_i \in \{m\}_s$. Note that the terms $\rho_{\rm st}^{(n)}$ with $n \notin \{m\}_s$ do not change.

B. Subsequent Ramsey measurements

As mentioned above, we start with the analysis of the second Ramsey measurement and then extend the results to subsequent measurements. To find the dynamics of operator $\mathfrak{R}(t)$ in the time interval $t_{\rm cyc} < t \leq t_{\rm cyc} + t_R^+$, we should take into account the fact that at time $t_{\rm cyc}$ the qubit undergoes a unitary transformation of rotation around the y axis, as seen from Hamiltonian (56). As a result, in the expression for $\mathfrak{R}(t)$, operator $\hat{I}_q + \sigma_z$ is transformed into $\hat{I}_q + \sigma_x$.

1. The contribution of term $\mathfrak{R}_{\rm st}$

The evolution of operator $\mathfrak{R}_{\rm st}(t)$ after the qubit rotation at $t_{\rm cyc}$ is described in exactly the same way as was done in Sec. VII B for $\rho(t)$. Indeed, $\mathfrak{R}_{\rm st}(t_{\rm cyc}^+)$ has the same form as the density matrix $\rho(0^+)$, Eq. (62), except that $\mathfrak{R}_{\rm st}$ has an extra factor r_1. Thus, the evolution of $\mathfrak{R}_{\rm st}(t)$ in the time interval $t_{\rm cyc} < t < t_{\rm cyc} + t_R$ is given by Eqs. (63) and (64) with the coefficients $C_{\lambda\varkappa}^{(n)}$ multiplied by r_1.

It follows from the above argument that if, after the next Ramsey rotation at $t_{\rm cyc} + t_R$, the transformed $\mathfrak{R}_{\rm st}$ [i.e., $\mathfrak{R}_{\rm st}(t_{\rm cyc} + t_R^+)$] is multiplied by $\hat{P}$ and the trace is taken over the qubit and TLSs, the result will be r_1^2. This is the contribution of $\mathfrak{R}_{\rm st}$ to $r_2(1)$.

a. Extending the result to $r_2(k)$ with $k > 1$. To find the contribution of $\mathfrak{R}_{\rm st}$ to $r_2(k)$ with $k > 1$, we note that, by applying the decomposition of the density matrix (63), one can write $\mathfrak{R}_{\rm st}(t_{\rm cyc} + t_R^+)$ as

$$\mathfrak{R}_{\rm st}(t_{\rm cyc} + t_R^+) = \mathfrak{R}_{\rm st}(t_R^+) + \hat{m}',$$

where $\hat{m}'$ is a sum of the terms proportional to σ_x, σ_y, and σ_z. Evaluating $r_2(k)$ involves resetting the qubit after each $k' t_{\rm cyc} + t_R^+$ with $k' < k$. After the reset, $\hat{m}'$ will go to zero. Therefore, by the end of the second cycle, $t \to 2t_{\rm cyc}$, we have $\mathfrak{R}_{\rm st}(2t_{\rm cyc}^-) = \mathfrak{R}_{\rm st}(t_{\rm cyc}^-) = \mathfrak{R}_{\rm st}(t_R^+)$. Operator $\mathfrak{R}_{\rm st}$ will evolve in the same way during the following cycles. The cycling does not change $\mathfrak{R}_{\rm st}$, that is, $\mathfrak{R}_{\rm st}(nt_{\rm cyc} + t_R^+) = \mathfrak{R}_{\rm st}(mt_{\rm cyc}^-)$ for any m and n. Therefore, the contribution of $\mathfrak{R}_{\rm st}$ to correlator $r_2(k)$ with $k > 1$ is the same as for $k = 1$. It is equal to r_1^2, independent of k.

2. The contribution of term $\mathfrak{R}_{\rm corr}$

Term $\mathfrak{R}_{\rm corr}$ describes the effect of correlations in the TLS dynamics on the outcome of the qubit measurements. To analyze this effect, we again start with the second Ramsey measurement, $k = 1$. We note first that the outcome of the qubit rotation at $t = t_{\rm cyc}$ can be written as

$$\hat{I}_q + \sigma_z \to \hat{I}_q + \sigma_z + \sum_{\alpha=\pm} \sigma_\alpha - \sigma_z. \tag{72}$$

We saw above that, after the rotation at $t_{\rm cyc} + t_R$, the last term, σ_z, is transformed into the terms that decay on reset; these terms also do not contribute to the trace over the qubit states if multiplied by $\hat{P}$. Therefore we do not consider the contribution from the term $\propto \sigma_z$ in $\mathfrak{R}_{\rm corr}(t_{\rm cyc}^+)$.

As seen from the master equation (59), the terms $\propto (\hat{I}_q + \sigma_z)\hat{\tau}_z^{m_1} \cdots \hat{\tau}_z^{m_s}$ in $\mathfrak{R}_{\rm corr}(t_{\rm cyc}^+)$ commute with the Hamiltonian and therefore do not lead to mixing of the qubit and TLS states. We denote this part of $\mathfrak{R}_{\rm corr}(t_{\rm cyc}^+)$ as $\mathfrak{R}'_{\rm corr}(t_{\rm cyc}^+)$. Over time t_R, operator $\mathfrak{R}'_{\rm corr}(t_{\rm cyc}^+)$ will decay as $\exp(-\sum_i W^{(m_i)} t_R)$. With the account taken of Eq. (71), after the Ramsey pulse at $t_{\rm cyc} + t_R$, $\mathfrak{R}'_{\rm corr}(t_{\rm cyc} + t_R^+)$ will

have the form of Eq. (70) in which $\hat{I}_q + \sigma_z$ is replaced by $\hat{I}_q + \sigma_x$ and the following replacement is also made:

$$\hat{\tau}_z^{(m_i)} \to \hat{\tau}_z^{(m_i)} \exp(-W^{(m_i)} t_{\rm cyc}), \qquad m_i \in \{m\}_s.$$

The trace of $\hat{P}\mathfrak{R}'_{\rm corr}(t_{\rm cyc} + t_R^+)$ over TLSs is zero; therefore, this term will not contribute to $r_2(1)$.

a. Extending the result to $r_2(k)$ with $k > 1$. Even though $\mathfrak{R}'_{\rm corr}(t_{\rm cyc} + t_R^+)$ does not contribute to $r_2(1)$, this term determines the values of $r_2(k)$ with $k > 1$. To see this, we first note that, after the qubit reset at $t_{\rm cyc} + t_R^+$, by time $2t_{\rm cyc}$, operator $\hat{I}_q + \sigma_x$ in $\mathfrak{R}'_{\rm corr}$ will transform into $\hat{I}_q + \sigma_z$ and there will emerge an extra factor $\exp[-\sum_{m_i} W^{(m_i)}(t_{\rm cyc} - t_R)]$ in the sum over $\{m\}_s$. Thus, $\mathfrak{R}'_{\rm corr}(2t_{\rm cyc}^-)$ will have the same structure as $\mathfrak{R}_{\rm corr}(t_{\rm cyc}^-)$. It is seen from Eq. (72) that this structure will be reproduced from cycle to cycle, so that

$$\mathfrak{R}'_{\rm corr}(kt_{\rm cyc}^-) = \frac{1}{2}(\hat{I}_q + \sigma_z) \sum_{s\geq 1} \sum_{\{m\}_s} \mathbb{K}_{\{m\}_s} \hat{\tau}_z^{(m_1)} \dots \hat{\tau}_z^{(m_s)} \times \exp\left[- \sum_{m_i \in \{m\}_s} W^{(m_i)}(kt_{\rm cyc} - t_R) \right] \prod_{n \notin \{m\}_s} \rho_{\rm st}^{(n)}. \tag{73}$$

Moreover, it is easy to see that $\mathfrak{R}_{\rm corr}(kt_{\rm cyc}^-) = \mathfrak{R}'_{\rm corr}(kt_{\rm cyc}^-)$ provided no measurements are done at $nt_{\rm cyc} + t_R^+$ with $0 < n < k$. This is because the terms $\propto \sigma_\pm$ in $\mathfrak{R}_{\rm corr}$ vanish on reset. Indeed, the rotation around the y axis at $nt_{\rm cyc} + t_R$ transforms $\sigma_\pm$ into $\sigma_x, \sigma_y, \sigma_z$ with different coefficients. All these components of the density matrix decay on reset.

The accumulation of the decay of different TLSs described by Eq. (73) ultimately determines the form of correlator $r_2(k)$. The very values of $r_2(k)$ are determined by the terms in $\mathfrak{R}_{\rm corr}(kt_{\rm cyc}^+)$, which are $\propto \sigma_\pm$ and emerge after transformation (72). They have to be studied separately for each product of the TLS operators $\hat{\tau}_z^{(m_1)}, \dots, \hat{\tau}_z^{(m_s)}$ in $\mathfrak{R}_{\rm corr}$. The analysis is similar to that in Sec. VII B and is described in Appendix F. The result is Eq. (19) for the centered correlator $\tilde{r}_2(k)$.

The described method allows one to calculate higher-order correlators as well. However, the expressions are cumbersome and will not be provided here. In Appendix A we describe an alternative approach to calculating probability r_1 and correlator $r_2(k)$, which is based on the properties of the telegraph noise that drives a qubit and mimics the coupling to TLSs.

IX. CORRELATORS OF MEASUREMENT OUTCOMES FOR GAUSSIAN FREQUENCY NOISE

We now consider the effect of Gaussian fluctuations of the qubit frequency $\delta\omega_q(t)$ on probability r_1 of the Ramsey measurement outcomes and their two- and three-time correlation functions $r_2(k), r_3(k, \ell)$. We express these probabilities in terms of the correlation functions f_n of phases θ_k accumulated by the qubit between the Ramsey pulses applied at times $kt_{\rm cyc}$ and $kt_{\rm cyc} + t_R$ with $k = 0, 1, \dots,$

$$\theta_k = \int_{kt_{\rm cyc}}^{kt_{\rm cyc}+t_R} \delta\omega_q(t)dt, \qquad f_k \equiv \langle \theta_n \theta_{n+k} \rangle;$$

cf. Eq. (2) (we use here the fact that, for a stationary noise, the elements of matrix $\langle \theta_n \theta_{n+k} \rangle$ depend only on k). Equation (36) relates correlators f_k to the power spectrum $S_q(\omega)$ of noise $\delta\omega_q(t)$. The probability distribution of the phases has the form

$$P(\{\theta\}) = Z^{-1} \exp\left[-\frac{1}{2} \sum_{m,n} (\hat{f}^{-1})_{n-m} \theta_n \theta_m \right], \qquad \sum_m (\hat{f}^{-1})_{n-m} f_{m-k} = \delta_{n,k}, \; f_k \equiv f_{n\,n+k} \tag{74}$$

where $\{\theta\}$ is the set of θ_n, while Z is the normalization factor.

The effect of classical noise can be easily described using the master equation approach. One does not have to care about the evolution of the TLS-dependent part of the density matrix, which significantly simplifies the calculation.

A. The first Ramsey measurement

We begin with the first cycle that starts at $t = 0$. Before the first Ramsey pulse is applied (the rotation around the y axis by $\pi/2$), the qubit is in the ground state. Its density matrix is

$$\rho(0^-) = (\hat{I}_q + \sigma_z)/2.$$

After the first Ramsey pulse at $t = 0$, we have $\rho(0^+) = (\hat{I}_q + \sigma_x)/2$. The evolution of the system at $0 < t < t_R$ is described by Eq. (64), in which one replaces the TLS operators by the numbers determined by the form of $\rho(0^+)$, i.e., $\rho_I \to 1, \rho_z \to -1, \rho_\pm \to 1$.

After the Ramsey pulse at $t = t_R$, we have, as seen from Eq. (67),

$$\hat{P}\rho(t_R^+) = \mathfrak{R}_0(t_R^+) + \hat{m}_0, \qquad \mathfrak{R}_0(t_R^+) = \tfrac{1}{2}(\hat{I}_q + \sigma_z) p(\theta_0), \tag{75}$$

where the probability $p(\theta)$ is given by the standard expression (7) and $\hat{m}_0$ is a sum of terms proportional to operators

$\sigma_{x,y,z}$. Taking a trace over the qubit states and averaging the result over phases θ using Eq. (74) gives Eq. (38) for

$$r_1 = \langle p(\theta_0)\rangle \equiv \int p(\theta_0)\prod_n d\theta_n P(\{\theta\})$$

(the integral goes over all θ_n for the correlated phases θ_n).

B. Repeated Ramsey measurements

If the averaging is not done after the first Ramsey measurement and instead the qubit is reset, term $\hat{m}_0$ in Eq. (75) will decay, whereas operator $\hat{I}_q + \sigma_z$, and thus $\mathfrak{R}_0(t_R^+)$, will not change. Then, by the end of the first cycle, $t \to t_{\rm cyc}$, operator $\rho(t_{\rm cyc}^-)$ will become $\mathfrak{R}_0(t_R^+) = \mathfrak{R}_0(t_{\rm cyc}^-) = p(\theta_0)\rho(0^-)$.

To describe the dynamics during the next cycle, we again use Eq. (63). The analysis is identical to that for the previous cycle, except that $\rho(0^-)$ is replaced with $p(\theta_0)\rho(0^-)$. After the pair of Ramsey pulses applied at $t_{\rm cyc}$ and $t_{\rm cyc} + t_R$, we have

$$\begin{aligned}\mathfrak{R}_0(t_{\rm cyc} + t_R^+) &= \mathfrak{R}_1(t_{\rm cyc} + t_R^+) + \hat{m}_1,\\ \mathfrak{R}_1(t_{\rm cyc} + t_R^+) &= \tfrac{1}{2}p(\theta_0)[\hat{I}_q - \sigma_z e^{-t_R/T_2}\cos(\phi_R + \theta_1)],\end{aligned} \tag{76}$$

where $\hat{m}_1$ has terms proportional only to σ_x and σ_y. Note that the random phase θ_1 has been accumulated over the time interval $(t_{\rm cyc}, t_{\rm cyc} + t_R)$, which is different from the time interval $(0, t_R)$ over which θ_0 was accumulated.

As a result of the reset during the time interval $(t_{\rm cyc} + t_R^+, 2t_{\rm cyc})$, by the end of the second cycle we again have $\mathfrak{R}_0(2t_{\rm cyc}^-) = p(\theta_0)\rho(0^-)$. The further evolution is just a repetition of the previous steps. After k pairs of Ramsey pulses, the expression for $\mathfrak{R}_0(kt_{\rm cyc} + t_R^+)$ will have the same form as Eq. (76) except that θ_1 will be replaced by θ_k.

To find the pair correlator $r_2(k)$, one has to multiply $\mathfrak{R}_0(kt_{\rm cyc} + t_R^+)$ by the projection operator $\hat{P}$, which gives, as seen by extending Eq. (76) from $t_{\rm cyc} + t_R^+$ to $kt_{\rm cyc} + t_R^+$,

$$\begin{aligned}\hat{P}\mathfrak{R}_0(kt_{\rm cyc} + t_R^+) &= \mathfrak{R}_2(kt_{\rm cyc} + t_R^+) + \hat{m}_2,\\ \mathfrak{R}_2(kt_{\rm cyc} + t_R^+) &= \tfrac{1}{2}\hat{I}_q p(\theta_0)p(\theta_k).\end{aligned} \tag{77}$$

Here, again, $\hat{m}_2$ is a sum of the terms proportional to σ_x, σ_y, and σ_z. Taking a trace over the qubit variables and averaging the result over the correlated phases θ_0, θ_k gives Eq. (38) for correlator $r_2(k) = \langle p(\theta_0)p(\theta_k)\rangle$.

To find the three-time correlator $r_3(k, \ell)$, we have to follow the evolution of operator $\mathfrak{R}_2(kt_{\rm cyc} + t_R^+)$ for the next $l - k$ cycles. There is no difference from the previous steps, as after reset we again express this operator in terms of the density matrix of the qubit in the ground state $\rho(0^-)$,

$$\mathfrak{R}_2[(k+1)t_{\rm cyc}^-] = p(\theta_0)p(\theta_k)\rho(0^-)$$

(we note that, as a result of the reset, operator $\hat{I}_q$ in $\mathfrak{R}_2$ goes into $\hat{I}_q + \sigma_z$). After $\ell - k$ cycles we have, similar to Eq. (77),

$$\begin{aligned}\hat{P}\mathfrak{R}_2(\ell t_{\rm cyc} + t_R^+) &= \mathfrak{R}_3(\ell t_{\rm cyc} + t_R^+) + \hat{m}_3,\\ \mathfrak{R}_3(\ell t_{\rm cyc} + t_R^+) &= \tfrac{1}{2}\hat{I}_q p(\theta_0)p(\theta_k)p(\theta_\ell).\end{aligned} \tag{78}$$

This leads to the expression $r_3(k, \ell) = \langle p(\theta_0)p(\theta_k)p(\theta_\ell)\rangle$. The explicit form of the centered correlator $\tilde{r}_3(k, \ell)$ in terms of correlators f_k for Gaussian noise is given in Eq. (39).

X. CONCLUSIONS

This paper describes several features of slow qubit frequency fluctuations that allow one to characterize the mechanism of the fluctuations. Of primary interest are fluctuations with the correlation time that exceeds the decoherence time of the qubit due to its decay and dephasing by fast processes. The approach is based on periodically repeated Ramsey measurements. Such measurements are fairly versatile, as one can vary the duration of the single measurement t_R, the period of the measurements $t_{\rm cyc}$, and the measurement phase ϕ_R that mimics the effect of the detuning of the drive from the mean qubit frequency. They are also advantageous as they enable finding the correlators of the measurement outcomes from a single data array.

Our results show that important information about the features of the frequency noise can be learned from the probability r_1 of observing "1" as a measurement outcome along with the two- and three-time correlation functions $r_2(k)$ and $r_3(k, \ell)$ of observing two "1s" separated by time $kt_{\rm cyc}$ and three "1s" separated by times $kt_{\rm cyc}$ and $\ell t_{\rm cyc}$, respectively. Correlators r_2 and r_3 determine the spectrum and the bispectrum of the measurement outcomes. They depend not only on the spectrum but also on the statistics of the qubit frequency noise.

The results cover a broad range of noise characteristics and sensitively depend on these characteristics. For TLSs, the relevant parameters include (i) the strength of the TLS coupling to the qubit (in units of frequency) compared to the TLS switching rates and to the reciprocal Ramsey accumulation time t_R^{-1}, (ii) the TLS asymmetry, i.e., the difference between the interstate switching rates, and last but not least, (iii) the number of TLSs coupled to the qubit. For Gaussian noise, the relevant noise characteristics are the intensity and the power spectrum; we have studied several major types of noise power spectra.

The developed analytical approach to describing the qubit dynamics during repeated Ramsey measurements is

quite general. It enables calculating probabilities r_1 and correlators $r_2(k)$ for dispersive coupling to TLSs, and also finding $r_{1,2,3}$ for Gaussian noise. The approach is recursive; it accounts for the evolution of the qubit during and between successive gate operations. It directly extends to studying higher-order correlators of the measurement outcomes. It can also be immediately extended to allow for gate errors and for measurement errors. For a qubit driven by telegraph noise, an alternative method of calculating correlators r_1 and $r_2(k)$ has been developed as well (Appendix A). Such noise mimics the effect of the coupling to independent TLSs.

The results of the simulations are in excellent quantitative agreement with the analytical results. Moreover, they allow us to study correlator r_3 for the coupling to TLSs, where analytical results become too cumbersome to be presented.

One of the central goals of the paper is to develop means for identifying whether noise is Gaussian. A distinguishing feature of Gaussian noise is the relation between the correlators. Once r_1 and $r_2(k)$ have been measured, they determine the form of $r_3(k,\ell)$. We use the corresponding relation to test noise "Gaussianity." We also find that the system can be "tuned" to be highly sensitive to non-Gaussianity by varying the measurement phase ϕ_R. In particular, for Gaussian noise, the centered correlator $\tilde{r}_3(k,\ell)$ is zero for $\phi_R = \pi/2$ independent of the noise spectrum and intensity.

Noise from TLSs is generally non-Gaussian. We illustrate this for the coupling to one TLS. One expects that noise would mimic Gaussian for weak coupling to a large number of TLSs. However, we find that, already for ten TLSs, and sometimes even for five TLSs, the noise can be close to Gaussian in a broad range from weak to strong coupling. This is only true, though, for symmetric TLSs. Noise from ten asymmetric TLSs is profoundly non-Gaussian even for a comparatively weak coupling. The asymmetry is seen, in particular, from a nonzero value of $\tilde{r}_3(k,\ell)$ for $\phi_R = \pi/2$.

Noise from TLSs is often assumed to be the cause of slow fluctuations of the qubit frequency. The presented analysis provides a tool for testing this assumption for various types of qubits. The developed methods can be extended to other types of noise of potential interest. In a way, this paper is a step toward creating a "map" of the effects of different types of slow qubit frequency fluctuations.

ACKNOWLEDGMENTS

We are grateful to Vadim Smelyanskiy for helpful and inspirational discussions and to Juan Atalaya, who participated in the work at an early stage. We also acknowledge useful discussions with Eleanor Rieffel and Lorenza Viola. F.W. and M.I.D. are thankful for the support from NASA Academic Mission Services, Contract No. NNA16BD14C, and from Google under NASA-Google SAA2-403512. M.I.D. acknowledges financial support from Google via PRO Unlimited.

APPENDIX A: EFFECT OF TELEGRAPH NOISE ON PERIODICALLY REPEATED RAMSEY MEASUREMENTS

In this section, we discuss an alternative method of deriving our major result in Eqs. (15) and (19) for the effect of the coupling to TLSs on the probability of a Ramsey measurement outcome and the correlator of the outcomes. We describe this effect as resulting from classical telegraph noise $\delta\omega_q(t)$ that is added to the qubit frequency. Noise comes from random uncorrelated switching of TLSs between their two states $|0\rangle^{(n)}$ and $|1\rangle^{(n)}$.

The method is based on relation (37) between the sought parameters r_1 and r_2 and the random phases

$$\theta_k = \int_{kt_{\rm cyc}}^{kt_{\rm cyc}+t_R} \delta\omega_q(t)dt$$

accumulated during the kth Ramsey measurement. The idea is to relate r_1, r_2 to the characteristic function of phases $\{\theta_k\}$.

The characteristic function is defined as the average over random phases θ_k,

$$\Phi(\vec{q}) = \langle e^{i\vec{q}\cdot\vec{\theta}}\rangle, \tag{A1}$$

where we consider the values $\theta_0, \theta_1, \ldots$ and numbers $q_1, q_2, \ldots$ as components of vectors $\vec{\theta} = (\theta_0, \theta_1, \theta_2, \ldots)$ and $\vec{q} = (q_0, q_1, q_2, \ldots)$.

From Eq. (7), r_1 and r_2 can be written in terms of the characteristic function as

$$r_1 = \tfrac{1}{2} + \tfrac{1}{2}e^{-t_R/T_2}\mathrm{Re}[e^{i\phi_R}\Phi(q_0 = 1, q_{k\neq 0} = 0)], \tag{A2}$$

$$\begin{aligned} r_2(k) = r_1^2 + \tfrac{1}{8}e^{-2t_R/T_2}\{&\Phi(q_0 = -1, q_k = 1, q_{k'\neq 0,k} = 0) \\ &- |\Phi(q_0 = 1, q_{k\neq 0} = 0)|^2 \\ &+ \mathrm{Re}[e^{2i\phi_R}\Phi(q_0 = 1, q_k = 1, q_{k'\neq 0,k} = 0) \\ &- e^{2i\phi_R}\Phi^2(q_0 = 1, q_{k\neq 0} = 0)]\}. \end{aligned} \tag{A3}$$

In what follows we derive explicit expressions for the characteristic function when the qubit frequency is subject to telegraph noise.

1. Characteristic function for one TLS

We first consider the case where the qubit is coupled to one classical TLS. Therefore, in this subsection we omit superscript (n) that enumerates TLSs; the TLS parameters

$V, W, \Delta W$ are the values of $V^{(n)}, W^{(n)}, \Delta W^{(n)}$ for the considered TLS. In particular, the qubit frequency shift due to the coupling to this TLS is $\delta\omega_q(t) = V(\tau_z(t) - \langle\tau_z\rangle)$. Here $\tau_z(t)$ is a classical random variable, telegraph noise that takes values ± 1 depending on whether the considered TLS is in state $|0\rangle$ or $|1\rangle$, i.e., τ_z is the eigenvalue of $\hat{\tau}_z$ on the corresponding states. It follows from the definition of θ_n that the characteristic function in Eq. (A1) can be written in the form

$$\Phi(\vec{q}) = \left\langle \exp\left[i \int_0^\infty \alpha(t)(\tau_z(t) - \langle\tau_z\rangle)dt \right] \right\rangle, \tag{A4}$$

where $\alpha(t)$ is a piecewise-constant function of time and is only nonzero in between the two Ramsey pulses within each cycle,

$$\alpha(t) = q_k V, \qquad kt_{\rm cyc} \le t \le kt_{\rm cyc} + t_R, \tag{A5}$$

whereas $\alpha(t) = 0$ for $kt_{\rm cyc} + t_R \le t \le (k+1)t_{\rm cyc}$.

a. Auxiliary functions

Telegraph noise $\tau_z(t)$ is a Markov process. The Markovian property and the feature that the noise takes values ± 1 allow one to derive an important relation [57], which extends to asymmetric TLSs and was previously obtained in Ref. [58] for symmetric TLSs,

$$\frac{d}{dt}\langle\tau_z(t)F[\tau_z]\rangle = -W\langle\tau_z(t)F[\tau_z]\rangle + \left\langle \tau_z(t)\frac{d}{dt}F[\tau_z] \right\rangle + \Delta W\langle F[\tau_z]\rangle, \tag{A6}$$

where $F[\tau_z]$ is an arbitrary functional of $\tau_z(t')$ for $0 \le t' \le t$, with $t = 0$ being the moment of imposing initial conditions. The last term in Eq. (A6) can be understood by noting that $\langle\tau_z\rangle = \Delta W/W$.

We use relation (A6) to reduce the calculation of the characteristic function $\Phi(\vec{q})$ to a set of ordinary differential equations. To this end, we introduce the following functions:

$$\chi(t) = \left\langle \exp\left[i \int_0^t \alpha(t')\tau_z(t')dt' \right] \right\rangle, \tag{A7}$$

$$\mathcal{X}(t) = \left\langle \tau_z(t) \exp\left[i \int_0^t \alpha(t')\tau_z(t')dt' \right] \right\rangle. \tag{A8}$$

From Eq. (A6), functions $\chi(t)$ and $\mathcal{X}(t)$ satisfy a system of coupled differential equations,

$$\frac{d}{dt}\chi(t) = i\alpha(t)\mathcal{X}(t), \tag{A9}$$

$$\frac{d}{dt}\mathcal{X}(t) = -W\mathcal{X}(t) + i\alpha(t)\chi(t) + \Delta W\chi(t), \tag{A10}$$

where we used the fact that ${\tau_z}^2 = 1$.

b. One-time characteristic function

With Eqs. (A9) and (A10) at hand, we are ready to derive the expression for $\Phi(q_0 = 1, q_{k\neq 0} = 0)$ in Eq. (A2), which we refer to as the one-time characteristic function.

It follows from Eqs. (A4) and (A7) that, to compute $\Phi(q_0 = 1, q_{k\neq 0} = 0)$, we simply need to compute $\chi(t)$, assuming that $\alpha(t) = V$ for $0 \le t \le t_R$ and $\alpha(t) = 0$ for $t > t_R$. For such $\alpha(t)$, we have

$$\Phi(q_0 = 1, q_{k\neq 0} = 0) = \chi(t_R)e^{-iVt_R\langle\tau_z\rangle}. \tag{A11}$$

Solving Eqs. (A9) and (A10) in the interval $0 \le t \le t_R$ with $\alpha(t) = V$, we find that

$$\begin{pmatrix} \chi(t_R) \\ \mathcal{X}(t_R) \end{pmatrix} = \hat{T}(V, t_R)\begin{pmatrix} \chi(0) \\ \mathcal{X}(0) \end{pmatrix}, \quad \begin{pmatrix} \chi(0) \\ \mathcal{X}(0) \end{pmatrix} = \begin{pmatrix} 1 \\ \Delta W/W \end{pmatrix}, \tag{A12}$$

$$\hat{T}(V, t_R) = \frac{1}{\gamma}\exp[-Wt_R/2]\begin{pmatrix} \frac{1}{2}W\sinh(\gamma t_R) + \gamma\cosh(\gamma t_R) & iV\sinh(\gamma t_R) \\ (iV + \Delta W)\sinh(\gamma t_R) & \gamma\cosh(\gamma t_R) - \frac{1}{2}W\sinh(\gamma t_R) \end{pmatrix}. \tag{A13}$$

Here we have introduced the transfer matrix $\hat{T}(V, t_R)$ that will be useful below. Carrying out the matrix multiplication in Eq. (A12), we obtain

$$\chi(t_R) = \Xi(t_R), \tag{A14}$$

where $\Xi(t_R)$ is given by Eq. (16) for $\Xi^{(n)}(t_R)$ for the considered nth TLS. Equations (A2), (A11), and (A14) give the expression for r_1, which coincides with Eq. (15) for the case of one TLS.

c. Two-time characteristic function

We now evaluate $\Phi(q_0 = \pm 1, q_k = 1, q_{k'\neq k,0})$ in Eq. (A3), which we refer to as the two-time characteristic functions. Again, we start with the case of the coupling

to one TLS. To this end, we need to solve Eqs. (A9) and (A10) for $\alpha(t)$ of the form

$$\alpha(t) = \pm V, \qquad 0 \le t \le t_R, \tag{A15a}$$
$$\alpha(t) = 0, \qquad t_R < t < kt_{\rm cyc}, \tag{A15b}$$
$$\alpha(t) = V, \qquad kt_{\rm cyc} \le t \le kt_{\rm cyc} + t_R. \tag{A15c}$$

The relevant two-time characteristic functions in Eq. (A3) are then expressed in terms of $\chi(t)$ as

$$\Phi(q_0 = \pm 1, q_k = 1, q_{k'\neq k,0} = 0) = \chi_{\pm}(kt_{\rm cyc} + t_R) e^{-i(q_0+q_k)Vt_R\langle\tau_z\rangle}, \tag{A16}$$

where subscript "±" corresponds to $\chi(t)$ calculated for $\alpha(t) = \pm V$ in the time interval $0 \le t \le t_R$, respectively.

Function $\chi_{\pm}(kt_{\rm cyc} + t_R)$ can be found using the transfer matrix in Eq. (A12) to connect the solutions of $\chi(t)$ in different regions where $\alpha(t)$ is a constant. The solution is reduced to just matrix multiplication,

$$\begin{pmatrix} \chi_{\pm}(kt_{\rm cyc} + t_R) \\ \mathcal{X}(kt_{\rm cyc} + t_R)) \end{pmatrix} = \hat{T}(V, t_R)\hat{T}(0, kt_{\rm cyc})\hat{T}(\pm V, t_R) \begin{pmatrix} \chi(0) \\ \mathcal{X}(0) \end{pmatrix}. \tag{A17}$$

This gives

$$\chi_+(kt_{\rm cyc} + t_R) = [\Xi(t_R)]^2 + [\xi_k(t_R)]^2,$$
$$\chi_-(kt_{\rm cyc} + t_R) = |\Xi(t_R)|^2 + |\xi_k(t_R)|^2, \tag{A18}$$

where $\xi_k(t_R)$ is given in Eq. (19). Substituting Eqs. (A16) and (A18) into Eq. (A3), for the pair correlator $r_2(k)$, we obtain the same expression as Eq. (19) written for the case of coupling to one TLS.

2. Characteristic function in the presence of multiple TLSs

Having found the characteristic function in the presence of one TLS, let us consider multiple independent TLSs. Qubit frequency noise is now a sum over TLSs, $\delta\omega_q = \sum_n V^{(n)}[\tau_z^{(n)} - \langle\tau_z^{(n)}\rangle]$.

A key advantage of using the characteristic function is that, in the presence of many independent TLSs coupled to the qubit, it factors into a product of the characteristic functions for individual TLSs. Specifically, the one-time characteristic function now becomes

$$\Phi(q_0 = 1, q_{k\neq 0} = 0) = \prod_n \chi^{(n)}(t_R) e^{-iV^{(n)}t_R\langle\tau_z^{(n)}\rangle} \tag{A19}$$

with $\chi^{(n)}(t_R)$ given in Eq. (A14) and the TLS parameters given by those of the nth TLS. Similarly, the expression for the two-time characteristic function reads

$$\Phi(q_0 = \pm 1, q_k = 1, q_{k'\neq k,0} = 0) = \prod_n \chi_{\pm}^{(n)}(kt_{\rm cyc} + t_R) e^{-i(q_0+q_k)V^{(n)}t_R\langle\tau_z^{(n)}\rangle} \tag{A20}$$

with $\chi_{\pm}^{(n)}(kt_{\rm cyc} + t_R)$ given in Eq. (A18).

Substituting Eqs. (A19) and (A20) into Eqs. (A2) and (A3), we immediately obtain the same expressions for r_1 and $\tilde{r}_2(k)$ as Eqs. (15) and (19).

APPENDIX B: SIMULATIONS

In this section we describe the algorithms used in the simulations of qubit frequency noise induced by two-level systems and of Gaussian qubit frequency noise.

1. Simulating noise from TLSs

Noise from TLSs is simulated as a sum of telegraph noises produced by each TLS independently. An nth TLS has two states, $|0\rangle^{(n)}$ and $|1\rangle^{(n)}$, in which its contributions to noise are 1 and -1, respectively. These contributions are multiplied by parameter $V^{(n)}$ of the coupling to the qubit to obtain the qubit frequency shift. The time is discretized with the same step δt for all TLSs. In the simulations we use $\delta t/t_R = 0.1$, where t_R is the duration of the Ramsey measurement. As everywhere else, we use the relative length of the cycle $t_{\rm cyc}/t_R = 3$

All TLSs are randomly (with equal probability) initialized in either the $|0\rangle$ or $|1\rangle$ state. At each time step a TLS can switch between its states $|0\rangle^{(n)}$ and $|1\rangle^{(n)}$. The switching probabilities are

$$p_{01}^{(n)} = W_{01}^{(n)}\delta t, \qquad p_{10}^{(n)} = W_{10}^{(n)}\delta t, \tag{B1}$$

where $W_{01}^{(n)}$ and $W_{10}^{(n)}$ are the switching rates. We numerically determine whether or not the TLS switches in a standard way by comparing $W_{ij}^{(n)}\delta t$ with a random number from the uniform distribution $U(0, 1)$.

The generated states of the TLS produce an array $d^{(n)}(m)$ of random numbers that take values ± 1. Here m enumerates the time steps. We collect $N = 10^5$ outcomes of the simulated Ramsey measurements, which means that we use $\tilde{N} = (t_{\rm cyc}/\delta t) \times 10^5$ samples, that is, $1 \le m \le \tilde{N}$. A kth Ramsey measurement, which is done in the time interval $kt_{\rm cyc} \le t \le kt_{\rm cyc} + t_R$, corresponds to the range of steps $k(t_{\rm cyc}/\delta t) < m \le k(t_{\rm cyc}/\delta t) + (t_R/\delta t)$. For our discretized time sequence, the random phase accumulated by the qubit in this time interval is

$$\theta_k = \sum_{m=1}^{\lceil t_R/\delta t\rceil} \sum_{n=1}^{N_{\rm TLS}} V^{(n)} d^{(n)}(\lfloor kt_{\rm cyc}/\delta t\rfloor + m). \tag{B2}$$

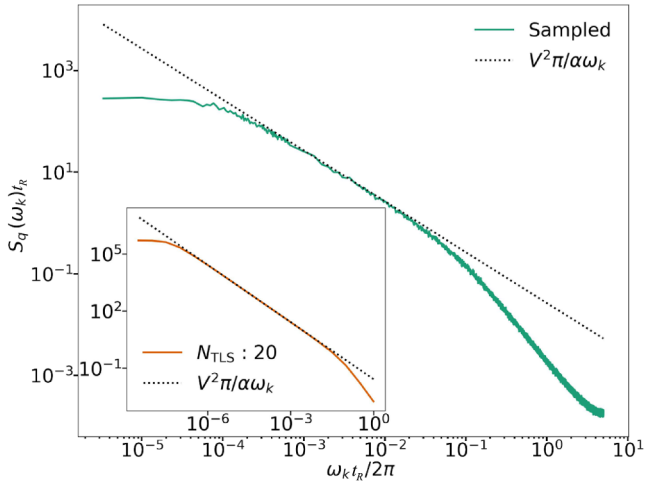

FIG. 8. Simulated power spectrum of the noise from ten symmetric TLSs with $V^{(n)} = V = 0.2/t_R$ and $W_{01}^{(n)} = W_{10}^{(n)} = \exp(-3n/4)/2t_R$ for $n = 1, 2, \ldots, 10$ (green data points). The spectrum displays $1/f$ character over more than two decades. The results agree with the analytical result, Eq. (14) of the main text. Inset: the power spectrum for 20 TLSs, $n = 1, \ldots, 20$, with the same V and $W_{ij}^{(n)}$ calculated from Eq. (14). In this case the spectrum displays more than five decades of $1/f$ behavior. The dashed lines in the main plot and in the inset show $1/f$ noise, $\alpha = 3/4$.

The probability of obtaining "1" in a kth measurement $p(\theta_k)$ is given by Eq. (7). We compare $p(\theta_k)$ with a random number o_k from $U(0,1)$. If $p(\theta_k) > o_k$, we set the outcome of the kth Ramsey measurement to $x_k = 1$; otherwise, we set $x_k = 0$. The whole procedure is independently repeated 300 times for statistical averaging. This allows us to numerically analyze and compare the parameters $r_1, r_2(k), r_3(k,\ell)$ with the theory, as well as to investigate other parameters of interest, as discussed in the main text.

Of primary interest to us is the analysis of TLSs that produce noise of $1/f$ type in a reasonably broad frequency range. There are many ways to obtain such noise. The results presented in the main text refer to noise in which the coupling of TLSs to the qubit is the same for all TLSs, $V^{(n)} = V$, but the distribution of the switching rates $W^{(n)} = W_{01}^{(n)} + W_{10}^{(n)}$ is log uniform. The noise spectrum is shown in Fig. 8.

The spectrum of the main plot in Fig. 8 is obtained from the simulated $d^{(n)}(m) = \pm 1$. At each time step m we evaluate the outcome

$$D(m) = \sum_{n=1}^{N_{\rm TLS}} V^{(n)} t_R d^{(n)}(m). \tag{B3}$$

The fast Fourier transform of $D(m)$ is then calculated in the standard way as

$$\tilde{D}(\omega_k) = \left| \sum_m \exp(-2\pi i m k/\tilde{N}) D(m) \right|^2 \Big/ \tilde{N}, \tag{B4}$$

where $\omega_k = 2\pi k/\tilde{N}$ and, as before, $\tilde{N} = N t_{\rm cyc}/\delta t$ with $N = 10^5$.

To obtain the power spectrum $S_q(\omega_k) = \langle \tilde{D}(\omega_k) \rangle$, this procedure is repeated 300 times to get sufficient statistics for averaging. For weak coupling to TLSs, spectrum $S_q(\omega)$ is immediately related to the centered correlator $\tilde{r}_2(k)$; cf. Sec. V

2. Simulating Gaussian noise

The effect of Gaussian noise on the outcomes of Ramsey measurements is fully characterized by the correlation function $f_k = \langle \theta_n \theta_{n+k} \rangle$ of phases θ_k acquired by the qubit in the measurements. Since the measurements are periodically repeated, one has to sample θ_k for successive k. The probability to have a given phase θ_k depends on the entire history of the previously "observed" phases $\theta_{k'}$ with $k' < k$. This means that the quantity of interest is the conditional probability

$$P(\theta_k|\theta_0, \ldots, \theta_{k-1}) = P(\theta_0, \ldots, \theta_k) \times [P(\theta_0, \ldots, \theta_{k-1})]^{-1}, \tag{B5}$$

where θ_0 is the outcome of the first measurement. Probability (B5) has to be evaluated recursively starting with the probability of θ_0. We use the fact that the distribution of the phases is stationary,

$$P(\{\theta\}) = Z^{-1} \exp\left[-\frac{1}{2} \sum_{k,k'} (\hat{f}^{-1})_{k-k'} \theta_k \theta_{k'} \right],$$

where Z is the normalization constant and $\hat{f}^{-1}$ is the matrix reciprocal to matrix $f_{kk'}$; we note that the matrix elements of the latter matrix are $f_{kk'} = f_{|k-k'|}$; cf. Eq. (74).

In evaluating the conditional probability given by Eq. (B5) one should keep in mind that the values of θ_k are correlated at a finite distance $k_{\rm corr}$, which is determined by the relation between the correlation time of the underlying noise and the period of the sequence $t_{\rm cyc}$. In other words, it means that, to a good approximation (which needs to be checked), $|f_k|$ can be set equal to zero for $k > k_{\rm corr}$. Then, for $k > k_{\rm corr}$, one can approximate the conditional probability $P(\theta_k|\theta_0, \ldots, \theta_{k-1})$ with $P(\theta_k|\theta_{k-k_{\rm corr}}, \theta_{k-k_{\rm corr}+1}, \ldots, \theta_{k-1})$, i.e., instead of probability (B5) we have to calculate

$$P(\theta_k|\theta_{k-k_{\rm corr}}, \ldots, \theta_{k-1}) = P(\theta_{k-k_{\rm corr}}, \ldots, \theta_k) \times [P(\theta_{k-k_{\rm corr}}, \ldots, \theta_{k-1})]^{-1}. \tag{B6}$$

It is important that all conditional probabilities in Eq. (B6) have a Gaussian form, albeit they are not zero mean, because of the correlations. As we now show, we can sample each θ_k from $\mathcal{N}(\mu_k, \sigma_k)$, where μ_k and σ_k are

respectively the mean value and the standard deviation for θ_k. They depend on the values of $\theta_{k'}$ with $k' < k$.

The first phase to be sampled, θ_0, is sampled with $\mu_0 = 0$ and $\sigma_0 = 1/\sqrt{f_0}$. To find the distribution of phases θ_k with $k > 0$, we note that, when calculating $P(\theta_{k-k_{\rm corr}}, \ldots, \theta_k)$, rather than using the full reciprocal matrix $(\hat{f}^{-1})_{|k-k'|}$ we should use a $(k_{\rm corr}+1) \times (k_{\rm corr}+1)$ matrix reciprocal to the $(k_{\rm corr}+1) \times (k_{\rm corr}+1)$ part of matrix $f_{kk'}$. This matrix $\Psi_{kk'}$ is defined by the equation

$$\sum_{m=k-k_{\rm corr}}^{k} \Psi_{km} f_{mk'} = \delta_{kk'}.$$

Along with $\Psi_{kk'}$ we need matrix $\psi_{kk'}$, which is the reciprocal of the $k_{\rm corr} \times k_{\rm corr}$ part of $f_{kk'}$,

$$\sum_{m=k-k_{\rm corr}}^{k-1} \psi_{km} f_{mk'} = \delta_{kk'}.$$

Matrices $\Psi_{kk'}$ and $\psi_{kk'}$ are symmetric. However, even though $f_{kk} = f_0$ is independent of k, the diagonal matrix elements of matrices Ψ_{kk} and ψ_{kk} depend on k.

There is an important relation between matrices $\hat{\psi}$ and $\hat{\Psi}$:

$$\psi_{kk'} = \Psi_{kk'} - (\Psi_{mk}\Psi_{mk'}/\Psi_{mm}),$$
$$k, k' = m - k_{\rm corr}, \ldots, m-1. \tag{B7}$$

This relation can be checked by multiplying from the left by $f_{k_1 k}$ and summing over $k = m - k_{\rm corr}, \ldots, m-1$.

Taking relation (B7) into account, we can write the exponential in $P(\theta_{k-k_{\rm corr}}, \ldots, \theta_k)$ as

$$\exp\left[-\frac{1}{2}\Psi_{kk}(\theta_k - \mu_k)^2 - \frac{1}{2}\sum_{m,m'=k-k_{\rm corr}}^{k-1} \psi_{mm'}\theta_m\theta_{m'} \right],$$

where

$$\mu_k = -\Psi_{kk}^{-1} \sum_{m=k-k_{\rm corr}}^{k-1} \Psi_{km}\theta_m \tag{B8}$$

is the phase accumulated over $k_{\rm corr}$ steps that preceded the kth step.

Ultimately, for the conditional probability of θ_k, we have the distribution

$$P(\theta_k|\theta_{k-k_{\rm corr}}, \theta_{k-k_{\rm corr}+1}, \ldots, \theta_{k-1})$$
$$= (\Psi_{kk}/2\pi)^{1/2} \exp\left[-\tfrac{1}{2}\Psi_{kk}(\theta_k - \mu_k)^2 \right]. \tag{B9}$$

We have also used here the Cramer rule that relates the matrix element Ψ_{kk} to the ratio of the determinants of matrices $\hat{\Psi}$ and $\hat{\psi}$.

The above prescription allows us to sample a sequence of random phases θ_k. Each obtained θ_k is used to determine whether the outcome of the simulated Ramsey measurement gives "0" or "1" based on probability (7). From the observed outcomes, we can calculate $r_1, r_2(k)$, and $r_3(k, \ell)$ as well as other statistical characteristics of the simulated sequence of periodic Ramsey measurements.

The value of $k_{\rm corr}$ depends on a particular type of noise. We choose it in such a way that the results become virtually independent of $k_{\rm corr}$. For exponentially correlated frequency noise with the correlation time $\tau_{\rm corr}$, one can choose $k_{\rm corr} = a_{\rm corr}\tau_{\rm corr}/t_{\rm cyc}$ with a sufficiently large $a_{\rm corr}$. For the $1/f$ -type noise we study, with the characteristic minimal frequency $\omega_{\rm min}$, one can choose $k_{\rm corr} = a_{1/f}\,(\omega_{\rm min}t_{\rm cyc})^{-1}$ with a sufficiently large $a_{1/f}$. However, for the parameters used in the simulations, we checked that the results become independent of $k_{\rm corr}$ once one sets $k_{\rm corr} \approx 10$ for the exponentially correlated noise and $k_{\rm corr} = 400$ for the $1/f$ noise.

APPENDIX C: EXPLICIT EXPRESSIONS FOR PHASE CORRELATORS FOR $1/f$ -TYPE NOISE

For completeness, here we provide the explicit expressions for correlators $f_k = \langle\theta_0\theta_k\rangle$ of the phases accumulated by the qubit during Ramsey measurements separated by k cycles, i.e., separated by time $kt_{\rm cyc}$. The expressions are related to the Gaussian noise $\delta\omega_q(t)$ produced by a large number of TLSs with the same coupling to the qubit and with the log-normal distribution of the switching rates. The power spectrum $S_q(\omega)$ of $\delta\omega_q(t)$ in this case is given by Eq. (46) in the main text.

The integral over ω, Eq. (36) in the main text, that relates f_k to $S_q(\omega)$ can be expressed in terms of the exponential integral and hyperbolic sine and cosine integral functions $\mathrm{Ei}(z)$, $\mathrm{shi}(z)$, and $\mathrm{chi}(z)$ as follows:

$$f_k = \frac{D_{\rm fl}\,t_R^2}{2\pi}\{2e^{-a_k b_{\rm min}}[(1-a_k b_{\rm min})[\cosh b_{\rm min} - 1]$$
$$+ b_{\rm min}\sinh b_{\rm min}]/b_{\rm min}^2$$
$$+ 2a_k^2\mathrm{Ei}(-a_k b_{\rm min}) - (a_k+1)^2\mathrm{Ei}(-a_k b_{\rm min} - b_{\rm min})$$
$$- (a_k-1)^2\mathrm{Ei}(b_{\rm min} - a_k b_{\rm min})\}, \qquad k > 0, \tag{C1}$$

and

$$f_0 = \frac{D_{\rm fl}t_R^2}{\pi}\left[-\frac{1}{b_{\rm min}^2} + \frac{2}{b_{\rm min}} - (b_{\rm min}-1)\exp(-b_{\rm min})/b_{\rm min}^2 \right.$$
$$\left. - \mathrm{chi}(b_{\rm min}) + \mathrm{shi}(b_{\rm min}) \right]. \tag{C2}$$

These expressions depend on two dimensionless parameters,

$$a_k = \frac{kt_{\rm cyc}}{t_R}, \qquad b_{\rm min} = \omega_{\rm min}t_R,$$

that are convenient for a numerical evaluation of correlators f_k.

APPENDIX D: THE EFFECT OF THE MEASUREMENT PHASE ϕ_R AND THE NUMBER OF TLSS

An important feature of Gaussian noise is that the centered correlator $\tilde{r}_3(k,\ell)$ is zero if phase ϕ_R of the Ramsey measurements is $\pi/2$. Testing the effect of the noise from TLSs for $\phi_R = \pi/2$ thus provides a glimpse at how different this noise is from Gaussian. In Fig. 9 we present the results of simulations of $\tilde{r}_2(k)$ and $\tilde{r}_3(k,\ell)$ for $\phi_R = \pi/2$ for the noise from ten TLSs with the same parameters as in the main text, where the simulations are done for $\phi_R = \pi/4$. As expected, correlators $\tilde{r}_2(k)$ display similar behavior to that for $\phi_R = \pi/4$ in Fig. 2. However, correlators $\tilde{r}_3(k,\ell)$ are extremely small for all values of $V^{(n)}$ that we study.

The noise from symmetric TLSs is close to Gaussian even for five TLSs provided they are symmetric. This is seen from Fig. 10. In contrast, the noise from asymmetric TLSs is profoundly non-Gaussian.

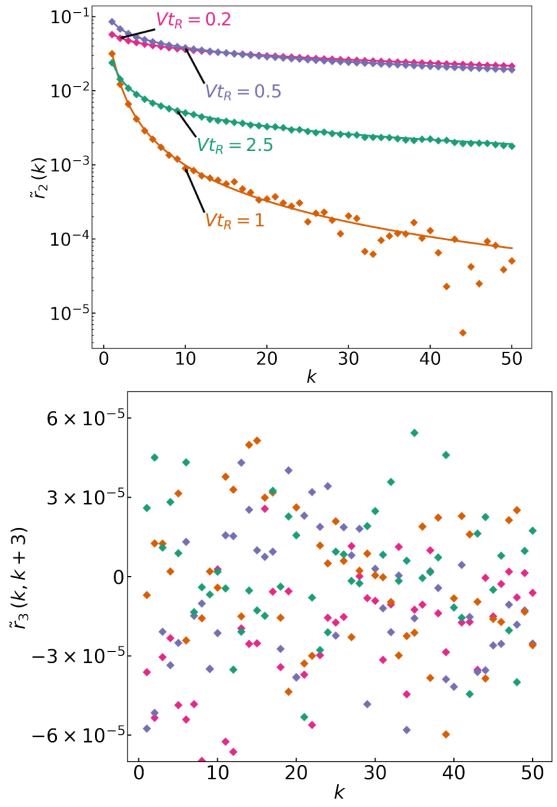

FIG. 9. Centered correlators $\tilde{r}_2(k)$ and $\tilde{r}_3(k,k+3)$ for ten symmetric TLSs for the measurement phase $\phi_R = \pi/2$. Top panel: ten TLSs with $W_{01}^{(n)}t_R = W_{10}^{(n)}t_R = \exp(-3n/4)/2$, $n = 1,\ldots,10$. The coupling is the same for all TLSs, $V^{(n)} = V$. The solid lines show the theory, Eq. (19). Correlators $\tilde{r}_3(k,\ell)$ display fluctuations around zero that cannot be resolved with 10^5 measurements.

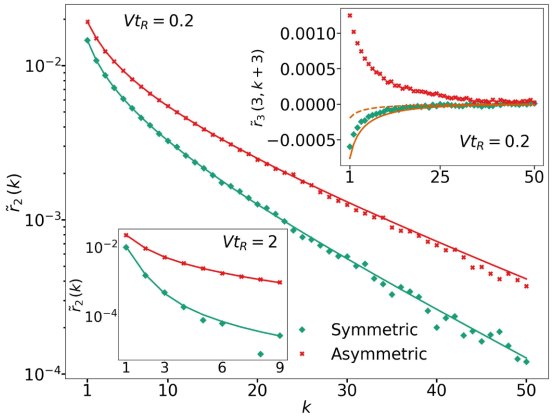

FIG. 10. Comparison of the effects of the coupling to symmetric and asymmetric TLSs, for 5 TLSs, $V^{(n)}t_R = 0.2$ and $\phi_R = \pi/4$. For the symmetric TLSs $W^{(n)}t_R = \exp(-3n/4)$ with $n = 1,\ldots,5$. For the asymmetric TLSs $W_{01}^{(n)}t_R = \exp[-3(n+1)]/4]/2$ and $W_{10}^{(n)}t_R = \exp(-3n/4)/2$. In the upper inset the lines are the Gaussian approximation for symmetric (solid) and asymmetric (dashed) TLSs.

APPENDIX E: TLS DYNAMICS DURING A RAMSEY MEASUREMENT

We consider here the dynamics of the TLS-dependent components of the density matrix during the Ramsey measurement, i.e., in the time interval $nt_{\rm cyc} < t < nt_{\rm cyc} + t_R$. These components, ρ_λ with $\lambda = I, z, \pm$, are defined in Eqs. (59) and (63). As indicated in the main text, the equations for ρ_λ with different λ are obtained by substituting Eq. (63) into the full master equation (60), multiplying the left- and right-hand sides by $\hat{I}_q, \hat{I}_q - \sigma_z, \sigma_\pm$, and taking a trace over the qubit states. The left-hand side of the resulting equation for ρ_λ is

$$\partial_t \rho_\lambda = \sum_n \sum_{\varkappa=0,z} \dot{C}_{\lambda\varkappa}^{(n)} \hat{\tau}_\varkappa^{(n)} \prod_{m\neq n} \sum_{\varkappa'=0,z} C_{\lambda\varkappa'}^{(m)} \hat{\tau}_{\varkappa'}^{(m)}. \tag{E1}$$

As seen from Eq. (60), the term $\sum_n \mathcal{L}^{(n)}\rho_\lambda$ on the right-hand side of the equation for $\partial_t\rho_\lambda$ has the same structure as Eq. (E1): a sum over n multiplied by the product over $m \neq n$ of $\sum_{\varkappa'=0,z} C_{\lambda\varkappa'}^{(m)} \hat{\tau}_{\varkappa'}^{(m)}$. The commutator $[\rho, H_{q-\rm TLS}]$ also has the same structure. One can divide both sides of the equation for $\partial_t\rho_\lambda$ by ρ_λ, reminiscent of the standard trick of separation of variables in a differential equation. This gives Eq. (65).

The equations for $C_{\lambda\varkappa}^{(n)}$ are split into sets of pairs of coupled equations. For $\lambda = I, z$, we have

$$\dot{C}_{\lambda 0}^{(n)} = 0, \qquad \dot{C}_{\lambda z}^{(n)} = \Delta W^{(n)} C_{\lambda 0}^{(n)} - W^{(n)} C_{\lambda z}^{(n)}, \qquad \Delta W^{(n)} = W_{10}^{(n)} - W_{01}^{(n)}. \tag{E2}$$

Parameter $\Delta W^{(n)}$ characterizes the asymmetry of the TLS, whereas $W^{(n)} = W_{10}^{(n)} + W_{01}^{(n)}$ is the TLS relaxation rate.

If $\lambda = +$, Eq. (65) for $C^{(n)}_{\lambda\varkappa}$ reads

$$\begin{aligned}\dot{C}^{(n)}_{+0} &= iV^{(n)}C^{(n)}_{+z},\\ \dot{C}^{(n)}_{+z} &= (\Delta W^{(n)} + iV^{(n)})C^{(n)}_{+0} - W^{(n)}C^{(n)}_{+z},\end{aligned} \tag{E3}$$

and, by construction, $C^{(n)}_{-\varkappa} = C^{(n)}_{+\varkappa}{}^{*}$.

Solving these equations, we obtain, for $\lambda = I, z$,

$$\begin{aligned}C^{(n)}_{\lambda z}(t) &= \left[C^{(n)}_{\lambda z}(0^+) - \frac{\Delta W^{(n)}}{W^{(n)}}C^{(n)}_{\lambda 0}(0^+)\right]e^{-W^{(n)}t}\\ &\quad + \frac{\Delta W^{(n)}}{W^{(n)}}C^{(n)}_{\lambda 0}(0^+),\\ C^{(n)}_{\lambda 0}(t) &= C^{(n)}_{\lambda 0}(0^+),\end{aligned} \tag{E4}$$

whereas

$$C^{(n)}_{+\varkappa}(t) = \sum_{k=1,2} B^{(k;n)}_{\varkappa}\exp(\nu^{(n)}_k t) \tag{E5}$$

with

$$\nu^{(n)}_{1,2} = -\tfrac{1}{2}W^{(n)} \pm \gamma^{(n)}, \tag{E6a}$$

$$\gamma^{(n)} = \tfrac{1}{2}[(W^{(n)})^2 + 4iV^{(n)}(\Delta W^{(n)} + iV^{(n)})]^{1/2}, \tag{E6b}$$

$$B^{(k;n)}_0 = [\nu^{(n)}_{3-k}C^{(n)}_{+0}(0^+) - iV^{(n)}C^{(n)}_{+z}(0^+)](\nu^{(n)}_{3-k} - \nu^{(n)}_k)^{-1}, \tag{E6c}$$

$$B^{(k;n)}_z = -i(\nu^{(n)}_k/V^{(n)})B^{(k;n)}_0, \qquad k = 1, 2. \tag{E6d}$$

These expressions are used in the main text to obtain $C^{(n)}_{\lambda\varkappa}(t)$ in the explicit form.

To find the initial conditions for the equations for $C^{(n)}_{\lambda\varkappa}$ in the above expressions, we take into account the fact that at instant $t = 0^+$ the qubit is in state $(|0\rangle + |1\rangle)/\sqrt{2}$, whereas the stationary TLS populations are given by Eq. (61). Therefore,

$$\begin{aligned}C^{(n)}_{Iz}(0^+) &= C^{(n)}_{\pm z}(0^+) = -C^{(n)}_{zz}(0^+) = \Delta W^{(n)}/2W^{(n)},\\ C^{(n)}_{I0}(0^+) &= C^{(n)}_{\pm 0}(0^+) = -C^{(n)}_{z0}(0^+) = \tfrac{1}{2},\end{aligned} \tag{E7}$$

With these initial conditions, we have, in particular,

$$\begin{aligned}C^{(n)}_{Iz}(t_R) &= -C^{(n)}_{zz}(t_R) = \Delta W^{(n)}/2W^{(n)},\\ C^{(n)}_{I0}(t_R) &= -C^{(n)}_{z0}(t_R) = \tfrac{1}{2},\end{aligned} \tag{E8}$$

and

$$\begin{aligned}C^{(n)}_{+z}(t_R) = \frac{1}{2}e^{-W^{(n)}t_R/2}\Bigg[&\frac{\Delta W^{(n)}}{W^{(n)}}\cosh(\gamma^{(n)}t_R)\\ &+ \left(i\frac{V^{(n)}}{\gamma^{(n)}} + \frac{\Delta W^{(n)}}{2\gamma^{(n)}}\right)\sinh(\gamma^{(n)}t_R)\Bigg];\end{aligned} \tag{E9}$$

the expression for $C^{(n)}_{+0}(t_R)$ is given in the main text, Eq. (16).

APPENDIX F: TIME EVOLUTION OF THE PAIR CORRELATOR

Operator $\mathfrak{R}_{\rm corr}$ defined in Eq. (70) describes the decay of the pair correlation function of the Ramsey measurement outcomes. Parameters $\mathbb{K}_{\{m\}_s}$ in the expression for $\mathfrak{R}_{\rm corr}$ read

$$\begin{aligned}\mathbb{K}_{\{m\}_s} = \frac{1}{2}e^{-t_R/T_2}\mathrm{Re}\Bigg[&e^{i\tilde{\phi}_R}\mathcal{J}^{(m_1)}\cdots\mathcal{J}^{(m_s)}\\ &\times\prod_{n\neq m_1,\ldots,m_s}\Xi^{(n)}(t_R)\Bigg],\end{aligned} \tag{F1}$$

where

$$\begin{aligned}\mathcal{J}^{(n)} &= C^{(n)}_{+z}(t_R) - \frac{\Delta W^{(n)}}{W^{(n)}}C^{(n)}_{+0}(t_R)\\ &= 2i\frac{V^{(n)}}{\gamma^{(n)}}\,\frac{W^{(n)}_{01}W^{(n)}_{10}}{W^{(n)2}}e^{-W^{(n)}t_R/2}\sinh\gamma^{(n)}t_R.\end{aligned} \tag{F2}$$

Here we have used Hamiltonian H_R, Eq. (57), in which ϕ_R was replaced by the auxiliary phase $\tilde{\phi}_R$ to compensate the coupling-induced shift of the average qubit frequency.

1. Time evolution of the terms $\propto \sigma_\pm$ in $\mathfrak{R}_{\rm corr}$

As indicated in the main text, the evolution of the terms $\propto \sigma_\pm$ in $\mathfrak{R}_{\rm corr}(t)$ in the time interval $kt_{\rm cyc} < t < kt_{\rm cyc} + t_R$ has to be studied separately for each term in the sum over $m_1, \ldots, m_s$ in $\mathfrak{R}_{\rm corr}(t)$. We denote the corresponding terms as $\mathfrak{R}_{\rm corr}(t|\{m\}_s)$,

$$\mathfrak{R}_{\rm corr}(t) = \sum_{s\geq 1}\sum_{\{m\}_s}\mathfrak{R}_{\rm corr}(t|\{m\}_s).$$

Similar to Eqs. (63) and (64), we seek $\mathfrak{R}_{\rm corr}(t|\{m\}_s)$ in the form

$$\begin{aligned}\mathfrak{R}_{\rm corr}(t|\{m\}_s) = \frac{1}{4}e^{-(t-kt_{\rm cyc})/T_2}\mathbb{K}_{\{m\}_s}\\ \times\sum_{\alpha=\pm}\sigma_\alpha\prod_n\sum_{\varkappa=0,z}\tilde{C}^{(n)}_{\alpha\varkappa}(t|\{m\}_s)\hat{\tau}^{(n)}_\varkappa.\end{aligned} \tag{F3}$$

The equations for coefficients $\tilde{C}^{(n)}_{\alpha\varkappa}(t|\{m\}_s)$ have the same form as Eq. (E3) for $C^{(n)}_{\alpha\varkappa}(t)$. The initial conditions for these equations are set at $t = t^+_{\rm cyc}$. They follow from expression (73) for $\mathfrak{R}_{\rm corr}(kt_{\rm cyc})$ and Eq. (72). They are different for the values of n that coincide with one of the components m_i of vector $\{m\}_s$ and for those values of n that differ from the

components of $\{m\}_s$. For the first group, we have

$$\tilde{C}^{(m_i)}_{+0}(kt^+_{\rm cyc}|\{m\}_s) = 0,$$
$$\tilde{C}^{(m_i)}_{+z}(kt^+_{\rm cyc}|\{m\}_s) = \exp[-W^{(m_i)}(kt_{\rm cyc} - t_R)], \quad m_i \in \{m\}_s. \tag{F4}$$

In contrast, for the second group, we have

$$\tilde{C}^{(n)}_{+0}(kt^+_{\rm cyc}|\{m\}_s) = 1/2,$$
$$\tilde{C}^{(n)}_{+z}(kt^+_{\rm cyc}|\{m\}_s) = \Delta W^{(n)}/2W^{(n)}, \qquad n \neq m_1, \ldots, m_s. \tag{F5}$$

It then follows from Eqs. (E4)–(E6) that

$$\begin{aligned}\tilde{C}^{(m_j)}_{+0}&(kt_{\rm cyc} + t_R|\{m\}_s)\\ &= i(V_{m_j}/\gamma^{(m_j)}) \sinh \gamma^{(m_j)} t_R\\ &\times \exp[-W^{(m_j)}(kt_{\rm cyc} - t_R/2)], \qquad m_j \in \{m\}_s, \end{aligned} \tag{F6}$$

whereas

$$\tilde{C}^{(n)}_{+0}(kt_{\rm cyc} + t_R|\{m\}_s) = \tfrac{1}{2}\Xi^{(n)}(t_R), \qquad n \notin \{m\}_s, \tag{F7}$$

where $\Xi^{(n)}(t_R)$ is given by Eq. (16).

At time $kt_{\rm cyc} + t_R$ the qubit undergoes a rotation about the z axis by an angle $\tilde{\phi}_R$ followed by a $\pi/2$ rotation about the y axis, as seen from Eqs. (56) and (57). As a result, the matrices σ_α in the operator $\mathfrak{R}_{\rm corr}(kt_{\rm cyc} + t_R|\{m\}_s)$, Eq. (F3), transform as

$$\sigma_\alpha \to e^{i\alpha\tilde{\phi}_R}(i\alpha\sigma_y - \sigma_z).$$

This transformation corresponds to the transformation of $\mathfrak{R}_{\rm corr}(kt_{\rm cyc} + t_R|\{m\}_s)$ into $\mathfrak{R}_{\rm corr}(kt_{\rm cyc} + t^+_R|\{m\}_s)$. As indicated in the main text, if the qubit is reset at $kt_{\rm cyc} + t^+_R$ then $\mathfrak{R}_{\rm corr}(kt_{\rm cyc} + t^+_R|\{m\}_s)$ decays. However, if the measurement is performed at time $kt_{\rm cyc} + t^+_R$, i.e., $\mathfrak{R}_{\rm corr}(kt_{\rm cyc} + t^+_R|\{m\}_s)$ is multiplied by $\hat{P} = (\hat{I}_q - \sigma_z)/2$ and the trace is taken over the qubit and TLSs, the contribution of $\mathfrak{R}_{\rm corr}(kt_{\rm cyc} + t^+_R|\{m\}_s)$ to the result of the measurement is

$$\tilde{r}_2(k) = \frac{1}{2}e^{-t_R/T_2} \times \sum_s \sum_{\{m\}_s} \mathbb{K}_{\{m\}_s} {\rm Re}\left[e^{i\tilde{\phi}_R}\prod_n 2\tilde{C}^{(n)}_{+0}(kt_{\rm cyc} + t_R|\{m\}_s)\right]. \tag{F8}$$

This result depends only on the coefficients $\tilde{C}^{(n)}_{+\varkappa}$ with $\varkappa = 0$, which describe the contribution of the identity operators of TLSs; the trace of the terms proportional to $\hat{\tau}^{(n)}_z$ is zero.

[1] Y. Nakamura, Yu. A. Pashkin, T. Yamamoto, and J. S. Tsai, Charge Echo in a Cooper-Pair Box, Phys. Rev. Lett. **88**, 047901 (2002).

[2] G. A. Álvarez and D. Suter, Measuring the Spectrum of Colored Noise by Dynamical Decoupling, Phys. Rev. Lett. **107**, 230501 (2011).

[3] J. Bylander, S. Gustavsson, F. Yan, F. Yoshihara, K. Harrabi, G. Fitch, D. G. Cory, Y. Nakamura, J.-S. Tsai, and W. D. Oliver, Noise spectroscopy through dynamical decoupling with a superconducting flux qubit, Nat. Phys. **7**, 565 (2011).

[4] D. Sank, R. Barends, R. C. Bialczak, Y. Chen, J. Kelly, M. Lenander, E. Lucero, M. Mariantoni, A. Megrant, M. Neeley, P. J. J. O'Malley, A. Vainsencher, H. Wang, J. Wenner, T. C. White, T. Yamamoto, Y. Yin, A. N. Cleland, and J. M. Martinis, Flux Noise Probed with Real Time Qubit Tomography in a Josephson Phase Qubit, Phys. Rev. Lett. **109**, 067001 (2012).

[5] F. Yan, J. Bylander, S. Gustavsson, F. Yoshihara, K. Harrabi, D. G. Cory, T. P. Orlando, Y. Nakamura, J.-S. Tsai, and W. D. Oliver, Spectroscopy of low-frequency noise and its temperature dependence in a superconducting qubit, Phys. Rev. B **85**, 174521 (2012).

[6] K. C. Young and K. B. Whaley, Qubits as spectrometers of dephasing noise, Phys. Rev. A **86**, 012314 (2012).

[7] G. A. Paz-Silva and L. Viola, General Transfer-Function Approach to Noise Filtering in Open-Loop Quantum Control, Phys. Rev. Lett. **113**, 250501 (2014).

[8] F. Yoshihara, Y. Nakamura, F. Yan, S. Gustavsson, J. Bylander, W. D. Oliver, and J.-S. Tsai, Flux qubit noise spectroscopy using Rabi oscillations under strong driving conditions, Phys. Rev. B **89**, 020503 (2014).

[9] M. Kim, H. J. Mamin, M. H. Sherwood, K. Ohno, D. D. Awschalom, and D. Rugar, Decoherence of Near-Surface Nitrogen-Vacancy Centers Due to Electric Field Noise, Phys. Rev. Lett. **115**, 087602 (2015).

[10] M. Brownnutt, M. Kumph, P. Rabl, and R. Blatt, Ion-trap measurements of electric-field noise near surfaces, Rev. Mod. Phys. **87**, 1419 (2015).

[11] P. J. J. O'Malley, *et al.*, Qubit Metrology of Ultralow Phase Noise Using Randomized Benchmarking, Phys. Rev. Appl. **3**, 044009 (2015).

[12] F. Yan, S. Gustavsson, A. Kamal, J. Birenbaum, A. P. Sears, D. Hover, T. J. Gudmundsen, D. Rosenberg, G. Samach, S. Weber, J. L. Yoder, T. P. Orlando, J. Clarke, A. J. Kerman, and W. D. Oliver, The flux qubit revisited to enhance coherence and reproducibility, Nat. Commun. **7**, 1 (2016).

[13] B. A. Myers, A. Ariyaratne, and A. C. B. Jayich, Double-Quantum Spin-Relaxation Limits to Coherence of Near-Surface Nitrogen-Vacancy Centers, Phys. Rev. Lett. **118**, 197201 (2017).

[14] C. M. Quintana, *et al.*, Observation of Classical-Quantum Crossover of $1/f$ Flux Noise and Its Paramagnetic Temperature Dependence, Phys. Rev. Lett. **118**, 057702 (2017).

[15] G. A. Paz-Silva, L. M. Norris, and L. Viola, Multiqubit spectroscopy of Gaussian quantum noise, Phys. Rev. A **95**, 022121 (2017).

[16] C. Ferrie, C. Granade, G. Paz-Silva, and H. M. Wiseman, Bayesian quantum noise spectroscopy, New J. Phys. **20**, 123005 (2018).

[17] C. Noel, M. Berlin-Udi, C. Matthiesen, J. Yu, Y. Zhou, V. Lordi, and H. Häffner, Electric-field noise from thermally activated fluctuators in a surface ion trap, Phys. Rev. A **99**, 063427 (2019).

[18] U. von Lüpke, F. Beaudoin, L. M. Norris, Y. Sung, R. Winik, J. Y. Qiu, M. Kjaergaard, D. Kim, J. Yoder, S. Gustavsson, L. Viola, and W. D. Oliver, Two-Qubit Spectroscopy of Spatiotemporally Correlated Quantum Noise in Superconducting Qubits, PRX Quantum **1**, 010305 (2020).

[19] G. Wolfowicz, F. J. Heremans, C. P. Anderson, S. Kanai, H. Seo, A. Gali, G. Galli, and D. D. Awschalom, Qubit guidelines for solid-state spin defects, Nat. Rev. Mater. **6**, 906 (2021).

[20] Y.-X. Wang and A. A. Clerk, Intrinsic and induced quantum quenches for enhancing qubit-based quantum noise spectroscopy, Nat. Commun. **12**, 6528 (2021).

[21] D. Ristè, C. C. Bultink, M. J. Tiggelman, R. N. Schouten, K. W. Lehnert, and L. DiCarlo, Millisecond charge-parity fluctuations and induced decoherence in a superconducting transmon qubit, Nat. Commun. **4**, 1913 (2013).

[22] K. Serniak, M. Hays, G. de Lange, S. Diamond, S. Shankar, L. D. Burkhart, L. Frunzio, M. Houzet, and M. H. Devoret, Hot Nonequilibrium Quasiparticles in Transmon Qubits, Phys. Rev. Lett. **121**, 157701 (2018).

[23] B. G. Christensen, C. D. Wilen, A. Opremcak, J. Nelson, F. Schlenker, C. H. Zimonick, L. Faoro, L. B. Ioffe, Y. J. Rosen, J. L. DuBois, B. L. T. Plourde, and R. McDermott, Anomalous charge noise in superconducting qubits, Phys. Rev. B 100, 140503 (2019).

[24] S. Schlör, J. Lisenfeld, C. Müller, A. Bilmes, A. Schneider, D. P. Pappas, A. V. Ustinov, and M. Weides, Correlating Decoherence in Transmon Qubits: Low Frequency Noise by Single Fluctuators, Phys. Rev. Lett. **123**, 190502 (2019).

[25] E. Paladino, L. Faoro, G. Falci, and R. Fazio, Decoherence and $1/f$ Noise in Josephson Qubits, Phys. Rev. Lett. **88**, 228304 (2002).

[26] Y. M. Galperin, B. L. Altshuler, and D. V. Shantsev, in *Fundamental Problems of Mesoscopic Physics*, edited by I. V. Lerner (Kluwer Academic Publishing, The Netherlands, 2004) pp. 141–165, comment: 18 pages, 8 figures, Proc. of NATO/Euresco Conf. "Fundamental Problems of Mesoscopic Physics: Interactions and Decoherence", Granada, Spain, Sept. 2003.

[27] L. Faoro and L. Viola, Dynamical Suppression of $1/f$ Noise Processes in Qubit Systems, Phys. Rev. Lett. **92**, 117905 (2004).

[28] Y. M. Galperin, B. L. Altshuler, J. Bergli, and D. V. Shantsev, Non-Gaussian Low-Frequency Noise as a Source of Qubit Decoherence, Phys. Rev. Lett. **96**, 097009 (2006).

[29] E. Paladino, Y. M. Galperin, G. Falci, and B. L. Altshuler, $1/f$ noise: Implications for solid-state quantum information, Rev. Mod. Phys. **86**, 361 (2014).

[30] C. Müller, J. H. Cole, and J. Lisenfeld, Towards understanding two-level-systems in amorphous solids: Insights from quantum circuits, Rep. Prog. Phys. **82**, 124501 (2019).

[31] Z. Huang, X. You, U. Alyanak, A. Romanenko, A. Grassellino, and S. Zhu, High-Order Qubit Dephasing at Sweet Spots by Non-Gaussian Fluctuators: Symmetry Breaking and Floquet Protection, Phys. Rev. Appl. **18**, L061001 (2022).

[32] B. Herzog and E. L. Hahn, Transient nuclear induction and double nuclear resonance in solids, Phys. Rev. **103**, 148 (1956).

[33] J. R. Klauder and P. W. Anderson, Spectral diffusion decay in spin resonance experiments, Phys. Rev. **125**, 912 (1962).

[34] F. Li, A. Saxena, D. Smith, and N. A. Sinitsyn, Higher-order spin noise statistics, New J. Phys. **15**, 113038 (2013).

[35] G. Ramon, Non-Gaussian signatures and collective effects in charge noise affecting a dynamically decoupled qubit, Phys. Rev. B **92**, 155422 (2015).

[36] L. M. Norris, G. A. Paz-Silva, and L. Viola, Qubit Noise Spectroscopy for Non-Gaussian Dephasing Environments, Phys. Rev. Lett. **116**, 150503 (2016).

[37] P. Szańkowski, G. Ramon, J. Krzywda, D. Kwiatkowski, and Ł. Cywiński, Environmental noise spectroscopy with qubits subjected to dynamical decoupling, J. Phys.: Condens. Matter **29**, 333001 (2017).

[38] Y. Sung, F. Beaudoin, L. M. Norris, F. Yan, D. K. Kim, J. Y. Qiu, U. von Lüpke, J. L. Yoder, T. P. Orlando, S. Gustavsson, L. Viola, and W. D. Oliver, Non-Gaussian noise spectroscopy with a superconducting qubit sensor, Nat. Commun. **10**, 3715 (2019).

[39] X. You, A. A. Clerk, and J. Koch, Positive- and negative-frequency noise from an ensemble of two-level fluctuators, Phys. Rev. Res. **3**, 013045 (2021).

[40] Z. A. Maizelis, M. L. Roukes, and M. I. Dykman, Detecting and characterizing frequency fluctuations of vibrational modes, Phys. Rev. B **84**, 144301 (2011).

[41] F. Sun, J. Zou, Z. A. Maizelis, and H. B. Chan, Telegraph frequency noise in electromechanical resonators, Phys. Rev. B **91**, 174102 (2015).

[42] F. Sakuldee and Ł. Cywiński, Spectroscopy of classical environmental noise with a qubit subjected to projective measurements, Phys. Rev. A **101**, 012314 (2020).

[43] A. Bechtold, F. Li, K. Müller, T. Simmet, P.-L. Ardelt, J. J. Finley, and N. A. Sinitsyn, Quantum Effects in Higher-Order Correlators of a Quantum-Dot Spin Qubit, Phys. Rev. Lett. **117**, 027402 (2016).

[44] N. A. Sinitsyn and Y. V. Pershin, The theory of spin noise spectroscopy: A review, Rep. Prog. Phys. **79**, 106501 (2016).

[45] R. C. Bialczak, R. McDermott, M. Ansmann, M. Hofheinz, N. Katz, E. Lucero, M. Neeley, A. D. O'Connell, H. Wang, A. N. Cleland, and J. M. Martinis, $1/f$ Flux Noise in Josephson Phase Qubits, Phys. Rev. Lett. **99**, 187006 (2007).

[46] T. Proctor, M. Revelle, E. Nielsen, K. Rudinger, D. Lobser, P. Maunz, R. Blume-Kohout, and K. Young, Detecting and tracking drift in quantum information processors, Nat. Commun. **11**, 5396 (2020).

[47] C. D. Wilen, S. Abdullah, N. A. Kurinsky, C. Stanford, L. Cardani, G. D'Imperio, C. Tomei, L. Faoro, L. B. Ioffe, C. H. Liu, A. Opremcak, B. G. Christensen, J. L. DuBois, and R. McDermott, Correlated charge noise and relaxation errors in superconducting qubits, Nature **594**, 369 (2021).

[48] C.-H. Liu, D. C. Harrison, S. Patel, C. D. Wilen, O. Rafferty, A. Shearrow, A. Ballard, V. Iaia, J. Ku, B. L. T. Plourde, and R. McDermott, Quasiparticle poisoning of superconducting qubits from resonant absorption of pair-breaking photons, ArXiv:2203.06577 (2022).

[49] P. W. Anderson, B. I. Halperin, and C. M. Varma, Anomalous low-temperature thermal properties of glasses and spin

glasses, Philos. Mag. J. Theor. Exp. Appl. Phys. **25**, 1 (1972).
[50] W. A. Phillips, Tunneling states in amorphous solids, J. Low Temp. Phys. **7**, 351 (1972).
[51] W. A. Phillips, Two-level states in glasses, Rep. Prog. Phys. **50**, 1657 (1987).
[52] T. Fink and H. Bluhm, Noise Spectroscopy Using Correlations of Single-Shot Qubit Readout, Phys. Rev. Lett. **110**, 010403 (2013).
[53] M. A. Nielsen and I. L. Chuang, *Quantum Computation and Quantum Information: 10th Anniversary Edition* (Cambridge University Press, Cambridge; New York, 2011).
[54] J. Bergli, Y. M. Galperin, and B. L. Altshuler, Decoherence in qubits due to low-frequency noise, New J. Phys. **11**, 025002 (2009).
[55] V. V. Dobrovitski, A. E. Feiguin, R. Hanson, and D. D. Awschalom, Decay of Rabi Oscillations by Dipolar-Coupled Dynamical Spin Environments, Phys. Rev. Lett. **102**, 237601 (2009).
[56] G. Ithier, E. Collin, P. Joyez, P. J. Meeson, D. Vion, D. Esteve, F. Chiarello, A. Shnirman, Y. Makhlin, J. Schriefl, and G. Schön, Decoherence in a superconducting quantum bit circuit, Phys. Rev. B **72**, 134519 (2005).
[57] S. Gurvitz, Generalized Landauer formula for time-dependent potentials and noise-induced zero-bias dc current, J. Phys. A: Math. Theor. **52**, 175301 (2019).
[58] V. E. Shapiro and V. M. Loginov, "Formulae of differentiation" and their use for solving stochastic equations, Phys. A: Stat. Mech. Appl. **91**, 563 (1978).